

1 Landsliding near Enguri dam (Caucasus, Georgia) and possible 2 seismotectonic effects 3

4 Alessandro Tibaldi ¹⁾, Paolo Oppizzi ²⁾, John Gierke ³⁾, Thomas Oommen ³⁾, Nino Tsereteli ⁴⁾, Zurab Gogoladze ⁴⁾

5 ¹⁾University of Milan Bicocca, Milan, Italy

6 ²⁾Geolog, Chiasso, Switzerland

7 ³⁾Michigan Technological University, Houghton, USA

8 ⁴⁾M. Nodia Institute of Geophysics, M. Javakishvili Tbilisi State University, Georgia

9 *Correspondence to:* Alessandro Tibaldi (alessandro.tibaldi@unimib.it)

10
11
12
13 **Abstract.** The Enguri dam and water reservoir, nested in southwestern Caucasus (Republic of Georgia), are surrounded by
14 steep mountain slopes. At a distance of 2.5 km from the dam, a mountain ridge along the reservoir is affected by active
15 deformations with a double vergence. The western slope, directly facing the reservoir, has deformations that involve a subaerial
16 area of 1.2 km². The head scarp intersects the main Jvari-Khaisi-Mestia road with offset of man-made features that indicate
17 slip rates of 2-9 cm/y. Static, pseudostatic and Newmark analyses, based on field and seismological data, suggest different
18 unstable rock volumes basing on the environment conditions. An important effect of variation of water table is showed, as
19 well as the possible destabilization of the landslide following seismic shaking compatible with the expected local Peak Ground
20 Acceleration. This worst scenario corresponds to an unstable volume in the order of up to $48 \pm 12 \cdot 10^6$ m³. The opposite,
21 eastern slope of the same mountain ridge is also affected by wide deformation involving an area of 0.37 km². Here, field data
22 indicate 2-5 cm/y of short-term and long-term slip rates. All these evidences are interpreted as resulting from two similar
23 landslides, whose possible causes are discussed, comprising seismic triggering, mountain rapid uplift, river erosion and lake
24 variations.

25
26 **Key words:** Caucasus, slope deformation, seismicity, Enguri dam

27 1 Introduction

28
29 GPS data and plate tectonic models indicate that the Greater and Lesser Caucasus are tectonically very active, with
30 ongoing mountain building processes comprising complex deformation with vertical and horizontal strain partitioning (Rebai
31 et al., 1993; Koçyiğit et al., 2001; Reilinger et al., 1997, 2006; Tan and Taymaz, 2006; Pasquaré et al., 2011). These processes
32 result from the still developing convergence and continent-continent collision between the Eurasian and Africa-Arabian plates
33 (Avagyan et al., 2010; Adamia et al., 2017) (Fig. 1). The active deformation is accompanied by diffuse seismicity that reaches
34 Ms of 6-7 (Tsereteli et al., 2016) and Intensity up to 10 (Varazanashvili et al., 2018) in the Caucasus in the Republic of Georgia.

35 In the southwestern part of the Georgian Greater Caucasus, there is the Enguri dam (the World's sixth highest dam) (Figs.
36 2 and 3A) that is part of the Enguri hydroelectric power station. This facility is the main hydroelectric plant of Georgia that

Formattato: Inglese (Stati Uniti)

Formattato: Non Apice/ Pedice

Formattato: Inglese (Stati Uniti), Non Apice/ Pedice

Formattato: Inglese (Stati Uniti)

Formattato: Italiano

Eliminato: numerical

Eliminato: Ground Penetrating Radar surveys of the head scarps confirm that these slip planes are steep and extend downward.

Eliminato: 2

41 presently furnishes the major part of the energy to the country. The Enguri dam is located nearby a series of geological features
42 that suggest Quaternary uplift, comprising deeply-entrenched rivers, deformed river terraces, recent faults and folds, and very
43 steep slopes (Tibaldi and Tsereteli, 2017; Tibaldi et al., 2017a). The strategic importance of the Enguri hydroelectric plant and
44 the fact that it is nested within one of the most tectonically active regions of Caucasus, suggest the necessity of carrying out
45 modern studies on the stability of the slopes surrounding the 19-km-long water reservoir, which are completely missing in the
46 scientific literature (only one technical consultant report exists, which is unpublished - CGS, 2015). Mountain slopes, in fact
47 are subject to gravity effects that can be enhanced by earthquake shaking (Gutierrez-Santolalla et al., 2005); it has been widely
48 demonstrated that this shaking can cause generation of shallow landslides and deep-seated gravity slope deformations
49 (DSGSDs) in active seismic areas (Beck, 1968; Solonenko, 1977; McCleary et al., 1978; Radbruch-Hall, 1978; Tibaldi et al.,
50 1995; McCalpin, 1999). The dynamic loading produced by seismicity may trigger discrete episodes of fast slope deformation
51 (e.g. Beck, 1968) or may accelerate already existing movements along DSGSD structures (e.g. Pasuto and Soldati, 1996).
52 Whether the movements are continuous (Varnes et al., 1989, 1990, 2000) or intermittent (Beget, 1985), the slopes under active
53 deformation pose a threat to infrastructures (Mahr, 1977; Radbruch-Hall, 1978; McCalpin and Irvine, 1995). Nearby the Enguri
54 reservoir there is also the important main road connecting the famous town of Mestia, hosting several ancient monuments and
55 a sky resort, with the rest of Georgia. This road is affected by important slope deformations in correspondence of the same
56 slope that faces the Enguri water reservoir. Moreover, in general, slope movements can turn into dangerous catastrophic
57 collapses, examples of which have been reported in Japan (Chigira and Kiho, 1994), Italy (Semenza and Ghirrotti, 2000) and
58 Canada (Evans and Couture, 2002).

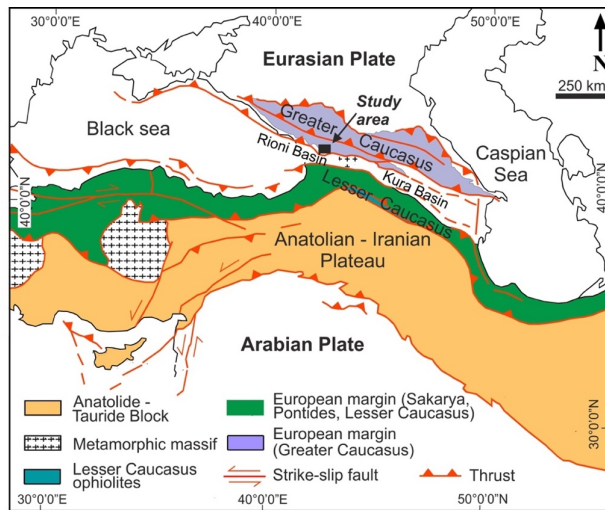
59 The present paper aims to describe, for the first time, the main active slope deformations affecting a mountain ridge that
60 runs along the eastern side of the Enguri water reservoir. The approach is multidisciplinary since it comprises geological,
61 geomorphological, ~~and structural surveys, completed with local seismic Peak Ground Acceleration calculation and analyses~~
62 of slope instability. The focus is to give the main first evidence that allows to define the boundaries of the unstable slopes,
63 their geometries, kinematics, slip rate and volume. Field observations are completed by preliminary 2-D numerical static,
64 pseudostatic and dynamic ~~analyses. 3-D modelling requires further extensive work that will be carried out in the future and~~
65 deserves a proper publication. The results show the presence of wide active slope deformations that interest the two opposite
66 slopes of this mountain ridge.

67 The paper has a series of main international impacts: i) it describes an outstanding example of intense gravity instability
68 with double vergence, ii) it contributes to answer to the challenging scientific questions on the causes that can increase the
69 instability of a slope facing a reservoir, and iii) it elucidates the regional processes that can contribute to induce intense slope
70 instability. The paper also iv) represents a contribution to assess the hydrogeologic hazard of the largest hydroelectrical facility
71 of Georgia.

Eliminato: and georadar

Eliminato: numerical modelling

Eliminato: modelling



75

76 **Figure 1: Tectonic map of the Arabia - Eurasia collision zone (modified from Sosson et al., 2010).**

77

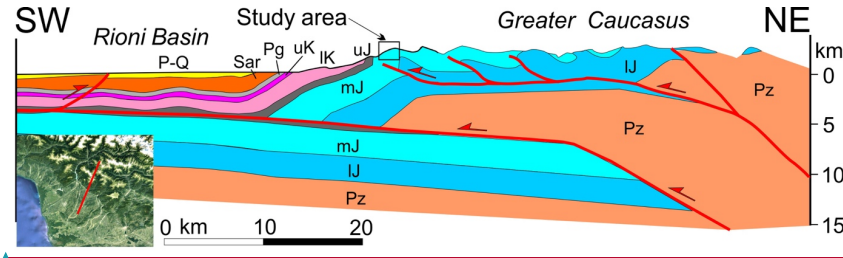
78 **2 Geological background**

79 The Greater and Lesser Caucasus are two fold-and-thrust belts separated by the Black Sea - Rioni basin and the South
 80 Caspian - Kura intermontane depression (Fig. 1) (Adamia et al., 1977, 2010; Banks et al., 1997; Mosar et al., 2010; Sosson et
 81 al., 2010). The Rioni and Kura regions first developed as foreland basins, in Oligocene-Early Miocene times, and successively
 82 were involved in the fold-and-thrust belts, representing an example of intra-plate, fast-growing mountain building process in
 83 Neogene times (Forte et al., 2010; Adamia et al., 2011; Alania et al., 2016). Fault-bend folds and fault-propagation folds are
 84 widespread with evidence of thin-skinned tectonics in both the Rioni and Kura fold-and-thrust belts (Adamia et al., 2010; Forte
 85 et al., 2010; Alania et al., 2016). Intense deformation involved these belts during the last 14-15 Ma, characterized by important
 86 fault slip along the main thrust systems that reached the greatest rate at the end of the Miocene (Adamia et al., 2017; Alania et
 87 al., 2016). These structural data are coherent with the results of apatite fission-track studies that revealed that the greatest
 88 exhumation rate occurred in the Miocene-Pliocene in the Greater Caucasus, although starting here in the Oligocene (Avdeev
 89 and Niemi, 2011; Vincent et al., 2007, 2011).

90 Successively, the mountain building processes continued up to the Quaternary as testified by geodetic and seismic data
 91 (Tsereteli et al., 2016). More in detail, historical and instrumental catalogues, seismic reflection sections, focal mechanism
 92 solutions, and field geological-structural surveys, show the presence of active compressional tectonics both in the core of the

93 Greater Caucasus as well as along the southern border and at the fold-and-thrust belts (Tsereteli et al., 2016; Tibaldi et al.,
94 2017a, 2017b). These authors showed that in the core of the Greater Caucasus there is a series of active reverse faults that are
95 parallel to the mountain range (i.e. WNW-ESE). They dip mostly towards NNE and display pure dip-slips. Along the southern
96 front of the Greater Caucasus, where the Enguri dam is located, there is a zone of active thrusting along planes dipping towards
97 NNE, as can be seen in the structural section portrayed in Figure 2. This section has been obtained by integrating geological-
98 structural field surveys from Tibaldi et al. (2017a) with geophysical and geological data from Banks et al. (1997). The section
99 shows the presence of a main basal thrust dipping north. The basal thrust has a ramp-flat geometry that produced a frontal
00 asymmetric ramp anticline in correspondence of the area studied here.

01



02

03 **Figure 2: Structural section passing through the study area (box), obtained by integrating our field surveys with**
04 **geophysical and geological data from Banks et al. (1997). Note the presence of a main basal thrust dipping north, which**
05 **shows a ramp-flat geometry that produced a frontal asymmetric ramp anticline.**

06

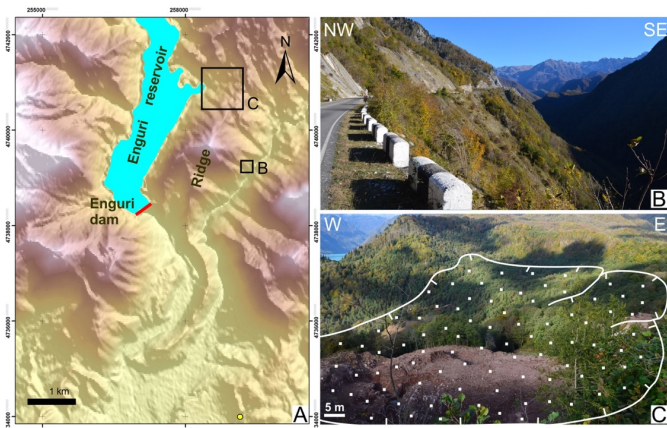
07 The Transcaucasus depression, located between the Greater and Lesser Caucasus, shows active inversion tectonics at part
08 of the Rioni Basin with uplift, folding, and faults mostly hidden under the youngest sedimentary cover (Tibaldi et al., 2017a,
09 2017b). The largest instrumental and historical earthquakes, with M_s 6-7, occurred both in the core of the two mountain belts
10 and along their fronts. Hypocenters are mostly located at depths < 30 km, with depths increasing eastward. A detailed new
11 assessment of historical earthquakes of all Georgia, assigns Intensity values up to 10 to the Caucasus region (Varazanashvili
12 et al., 2018). These data are consistent with geodetic observations by Reilinger et al. (2006), which indicate a total convergence
13 rate of 2-3 cm/y between the plates located south and north of the Caucasus. The same authors suggest that about 1/3 of this
14 convergence is accommodated along the Caucasus by crustal shortening. The total post-collisional sub-horizontal shortening
15 of this mountain belt caused by the northward motions of the Africa-Arabian plate is estimated at hundreds of kilometers
16 (Barrier and Vrielynck, 2008; Meijers et al., 2013).

17 From a stratigraphic and lithological point of view, pre-Mesozoic basement and Jurassic sedimentary rocks characterize
18 the axial zone of the Greater Caucasus, whereas Cretaceous and Cenozoic sedimentary rocks are present in the more external
19 zones (Adamia et al., 2011; Mosar et al., 2010). At the foot of the southwestern Greater Caucasus, where the Enguri dam is

Eliminato: .

Formattato: Tipo di carattere:(Predefinito) Times New Roman, 10 pt, Colore carattere: Nero

21 located, carbonatic deposits dominate together with rarer terrigenous and tuffaceous rocks of volcanic origin. More detailed
22 data on the local geology are given below.
23



24
25 **Figure 3:** A. DEM of the Enguri dam area. Boxes locate Figures 3B and 3C. B. Segment of the Jvari-Khaishi-Mestia
26 road where it crosses the eastern slope of the ridge highlighted in Figure 3A; here rocks and slopes are very steep, up
27 to 70°. C. Oblique view (looking north) of the area, facing the Enguri water reservoir, affected by active slope
28 deformation. The scale is referred only to the forefront zone.

29

30 3 Results

31 3.1 Local geology and geomorphology

32 The studied area shows the presence of Jurassic volcanic and terrigenous rocks and Cretaceous carbonatic deposits
33 generally dipping to the south (Fig. 4). Cretaceous strata crop out around the Enguri dam where they dip mostly at 60-70° (Fig.
34 3B), whereas they become steeper southward, assuming a vertical dip near the Rioni plain, accompanied by local overturning
35 of the strata with a steep dip to the north. Strata assume a gentler inclination northward, becoming up to subhorizontal towards
36 the northern part of the Enguri reservoir. The region is affected by faults and folds that make the structural architecture locally
37 more complicated. North of the Enguri dam, below the carbonatic strata, there are also Jurassic deposits made of sandstones,
38 tuffs, tuff-breccia and gypsum layers that locally crop out along the southeastern side of the artificial water reservoir (Fig. 4).
39 Their dip is again dominantly towards southeast and south, and generally becomes gentler northward, in the order of 15-40°.

40 From a geomorphological point of view, the studied area is characterised by the presence of two parallel river valleys
41 trending about N-S (Fig. 3A). The western valley hosts the Enguri dam, whereas the eastern valley is deeply entrenched with

Eliminato: 2
Eliminato: 2
Eliminato: 2
Eliminato: 2

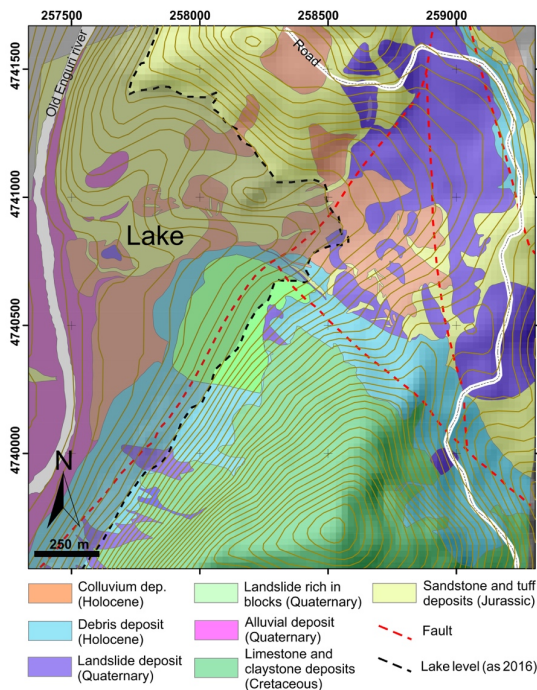
Eliminato: 3
Eliminato: 2

Eliminato: 3

Eliminato: 2

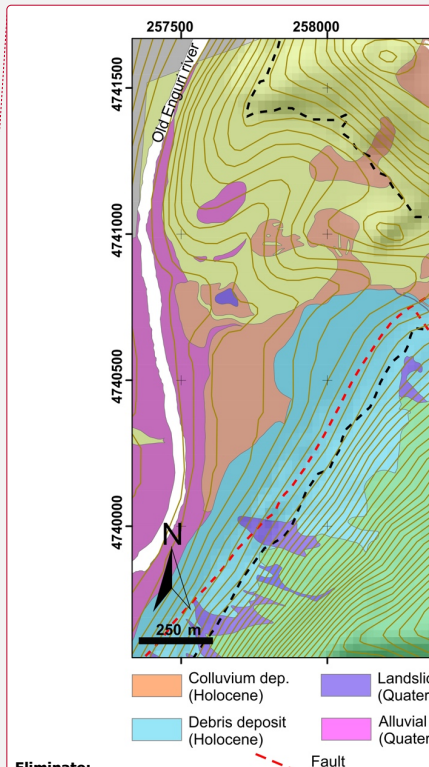
50 differences of altitudes between the valley bottom and the mountain ridge up to 700 m. These two valleys are separated by an
 51 about 9-km-long mountain ridge whose western slope constitutes the side of the artificial water reservoir. The two opposite
 52 slopes of the mountain ridge are very steep, reaching up locally an inclination of 70° linked with the presence of outcropping
 53 carbonatic rocks steeply dipping southward. The Jvari-Khaishi-Mestia main road runs along this mountain ridge and is under
 54 the threat of small landslides and, especially, of rolling stones at several sites, in particular where the road comes across the
 55 outcropping steep rock strata (Fig. 3B).

56 This road is also affected by deformations related to the presence of the active head scarps of the two landslides that
 57 characterize the opposite slopes of the 9-km-long mountain ridge. The main head scarp of the landslide facing west, towards
 58 the Enguri reservoir, is represented in the upper part of Figure 5. The head scarp of the other landslide is represented in the
 59 same Figure 5 on the slope facing east.

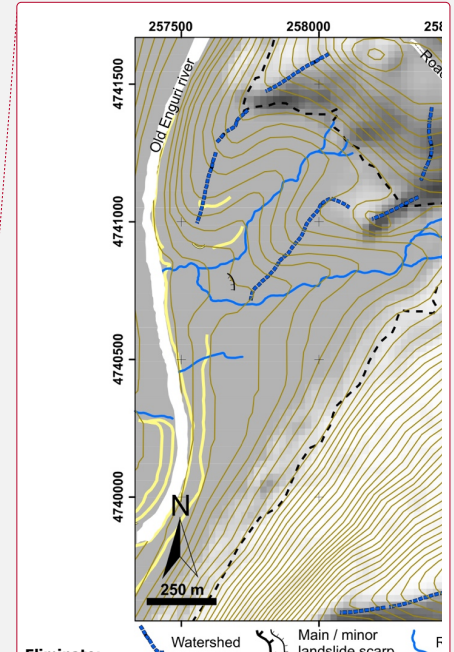
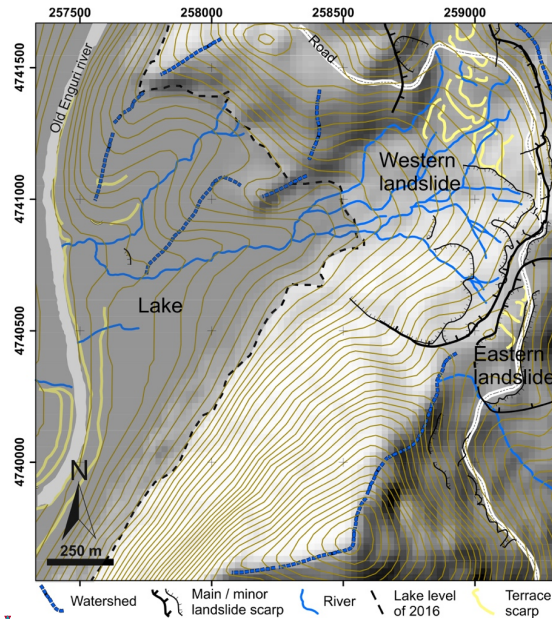


60
 61 **Figure 4:** Geological map of the area surrounding the western landslide, based on our new field surveys in the onshore
 62 zone and data from Zolotarev et al. (1968) for the zone now submerged by the Enguri water reservoir.

Eliminato: 2
 Formattato: Rientro: Prima riga: 0,75 cm



Eliminato:
 Formattato: Tipo di carattere:(Predefinito) Times New Roman, 10 pt, Colore carattere: Nero
 Eliminato: 3



Eliminato:

Formattato: Tipo di carattere:(Predefinito) Times New Roman, 10 pt, Colore carattere: Nero

Eliminato: 4

Eliminato: 2

Eliminato: 4

Eliminato: 4

67
68 **Figure 5: Geomorphological map of the area surrounding the western landslide, based on our new field surveys in the**
69 **onshore zone and data from Zolotarev et al. (1968) for the zone now submerged by the Enguri water reservoir. The**
70 **main head scarp of the other landslide facing east, is also represented.**

3.2 Morphostructural field evidence of the western landslide

73 The western slope of the mountain ridge faces directly the Enguri water reservoir. At a distance of about 2.5 km from the
74 Enguri dam, this slope shows a series of landforms typical of recent/active deformation: along the Jvari-Khaishi-Mestia road,
75 at an altitude of 720-740 m, there is a series of scarps facing westward (Figs. 3C and 5). They have a sinuous shape in plan
76 view, given by anastomosed single scarps with a westward concave side. This suggests that these features resulted from joining
77 a series of discrete head scarps. Each scarp is from a minimum of 20 m up to 70 m high. At the scarp foot, the slope is from
78 sub-horizontal to gentle dipping westward (average inclination = 17°), whereas several changes of inclination are present along
79 the slope. These changes are highlighted as terrace scarps in Figure 5; they have been checked in the field and do not correspond
80 to man-made features. Most of these scarps are oriented perpendicularly to the local slope dip and are located in the upper part

86 of the slope. These data suggest they may represent secondary ruptures within a moving slope. This is further confirmed by
87 the presence of several tilted trees, with local zones where 100% of trunks are tilted, all along the area highlighted in Figure
88 3C.

Eliminato: 2

89 In regard to river streams, they have been outlined based on the present network and topographic maps surveyed before
90 the formation of the water reservoir. Rivers mostly run along the average slope dip down to about half of the original slope
91 with a dendritic pattern (Fig. 5). At the lower half of the slope, now completely covered by the lake, one single river was
92 draining the landslide area. A few river anomalies are present: at the foot of the slope, now under the lake, the lowermost
93 segment of the aforementioned single river was running parallel to the main Enguri river but with a northward flow. In the
94 northern, upper part of the slope affected by the landslide, one short river segment runs perpendicular to the average slope dip.
95 These river diversions may correspond to anomalies in the average slope topography.

Eliminato: 4

96 In regards to fractures and fissures, these affect all the area close to the head scarps. The asphalted surface of the Jvari-
97 Khaishi-Mestia road, here is affected by several offsets: deformation is represented by fissures, up to a few cms wide, and
98 scarps facing westwards (Fig. 6). These structures are parallel to sub-parallel to the morphological head scarps. The scarps
99 offsetting the road have been repeatedly measured from November 2015 to May 2017, showing a vertical component of offset
00 up to 14 cm developed during this time frame, giving an average slip rate of 9.3 cm/y at the northernmost, fastest structure. As
01 an example, in Fig. 6B we report the northern scarp surveyed on November 2015, that was 11 cm high; the same scarp then
02 increased to 20 cm in May 2016 (Fig. 6C).

Eliminato: 5

Eliminato: 5

Eliminato: 5

03 In the southern segment of the head scarps, a detailed survey in the forest showed the presence of tens of meters long,
04 and up to 3.8 m wide fissures (e.g. Fig. 6D). All the fissures are vegetated and mostly filled, with local presence of trees grown
05 inside the fissure, with trunks of about 20 cm in diameter. The bottom of the fissures is filled by coarse debris and soil, while
06 the empty upper part of the fissures has a depth in the range of 1-3 m. This suggests that these fissures have a long history, at
07 least of some tens of years. The area at the foot of this fissure swarm is locally known as Khoko landslide. Presently, gypsum
08 is here excavated at a small open mine for economic reasons (Fig. 6A). At the foot of this landslide, nearby the coast of the
09 artificial water reservoir, we recognized the presence of intensely deformed gypsum rocks (Fig. 6E).

Eliminato: 5

Eliminato: 5

Eliminato: 5

10 We opened two trenches across some of the main active scarps affecting the Jvari-Khaishi-Mestia road (Fig. 7). The
11 trenches show evidence of repeated downthrown of the western block. The western part of Trench 1, in fact, contains two
12 buried old road surfaces: the oldest is lowered of 1.3 m respect to the present road level, whereas the second one is lowered of
13 20 cm (Fig. 7C). Interviews with local inhabitants indicated that the oldest road was made during the Soviet era, about AD
14 1960 ± 5 ys. Although we are aware that the Soviet road was narrower than the present one, the presence of filling material
15 between the various road levels indicates that subsidence here did occur since it was necessary to restore the road plane level.
16 Also at nowadays, in fact, continuous road maintenance is here necessary with tens of centimeters of asphalt added above the
17 downhill segment of the road surface to maintain the level. Trench 2 also contains two buried roads, plus a level of collapsed
18 trees and pieces of woods that is offset by several slip planes dipping downslope (Fig. 7D).

Eliminato: 6

Eliminato: 6

Eliminato: 6

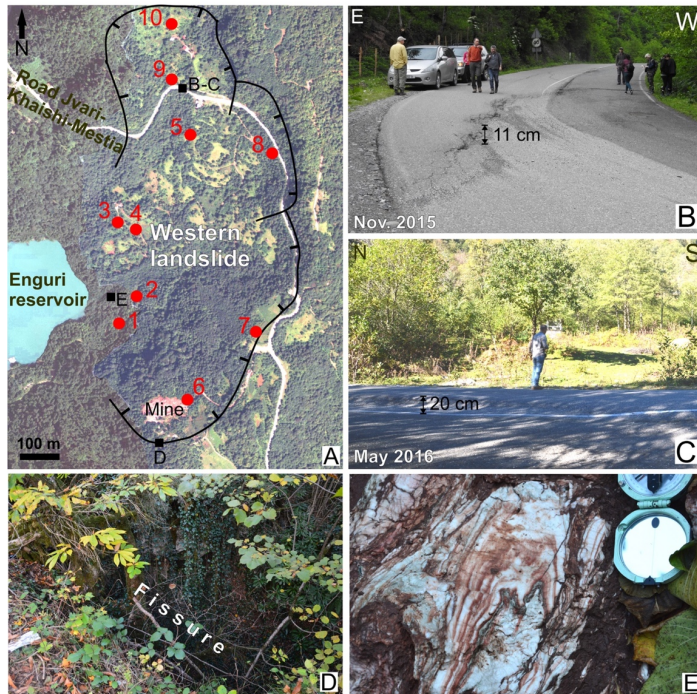
30 The total subaerial area affected by slope deformation is of 1.2 km². The slip surface is not unique and probably there are
31 different, partially superimposed slip planes as suggested by the complexity of the head scarps and of slope morphology, and
32 the dimension of the whole unstable slope. All the piezometers installed during 2015 across the landslide body, are broken at
33 depths between 16 and 49 m, as can be appreciated by comparing columns 6th and 8th in Table 2. These widespread ruptures
34 should correspond to the depth of some active slip planes. Other logs anyway, drilled during the Soviet era (see the section on
35 [slope stability analyses](#)), suggest that the intact substrate rock is located at deeper levels. This can be seen, for example, in the
36 logs n. 3261 and 3297 (drilled in 1966) (Fig. 8). These logs show the presence of clastic, unconsolidated deposits, rich in clay
37 and locally gypsum fragments, down to a depth of 57.5 m (log 3297), and/or clastic deposits with a silt to clay matrix down to
38 at least 61 m (log 3297) and at least 80 m (log 3261). Other logs, such as n. 3291 (drilled in 1966), indicate clay and gypsum
39 deposits down to a depth of 30 m, below which there is the substrate. These observations, together with detailed geological
40 and geomorphological surveys, allowed to prepare the geological vertical section shown in Figure 8B, which in turn is the
41 base to construct the geotechnical section used for [slope stability analyses](#). The geological section indicates that the intact
42 substrate rock is located at a variable level, always deeper than 30 m and locally even > 80 m.

Eliminato: numerical modelling

Eliminato: 7

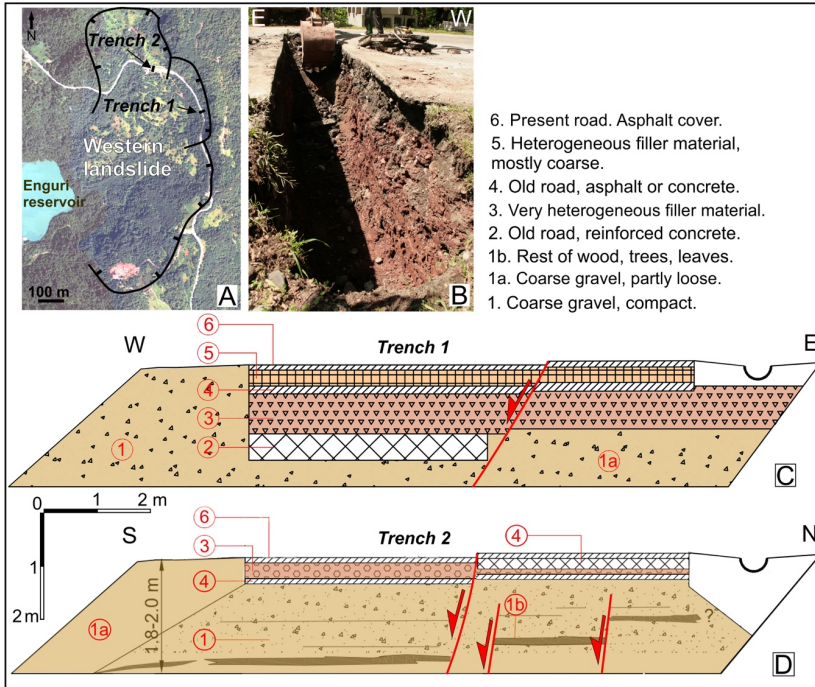
Eliminato: 7

Eliminato: numerical modelling of



47
 48 **Figure 6.** A. Black lines show the main head scarps of the unstable slope area facing the Enguri reservoir. Black boxes
 49 locate Figures B-E. Red dots are location of piezometers discussed in the modelling section. B. and C. Photos of one of
 50 the several slip planes that offset the Jvari-Khaishi-Mestia road, taken in November 2015 and May 2016 respectively;
 51 note the large increase of offset. D. NE-SW-striking fissure located at the head scarp of the southern part of the unstable
 52 slope area. E. Strongly deformed gypsum deposits located at the foot of the northern part of the unstable slope area.
 53

Eliminato: 5



55

56

57

58

59

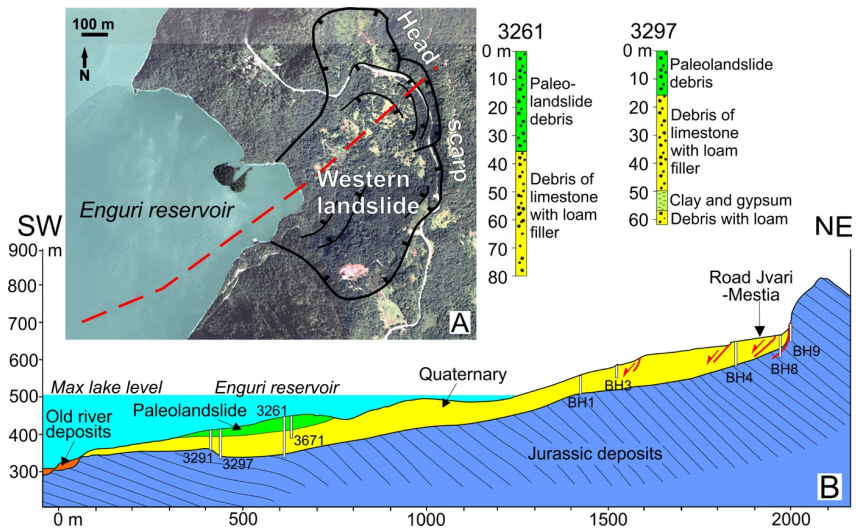
60

61

Figure 7: A. Location of the trenches at the northern part of the unstable slope facing the Enguri reservoir. B. Photo of Trench 2 opened across one of the main active scarps affecting the Jvari-Khaishi-Mestia road, location in Figure 7A. C. and D. Logs of the northern and western wall of Trench 1 and 2, respectively. Numbers refer to the legend. Present and old, offset roads are white. The oldest road is downthrown to the west of 1.3 m. The red lines show the location of shallow active slip planes.

Eliminato: 6

Eliminato: 6



64
65
66 **Figure 8:** A. Trace (red line) and B. geological section across the slope facing the Enguri reservoir. White columns
67 represent locations and depth of logs used to construct the cross section. Data of the submerged part derived from
68 geological surveys made at the Soviet era before dam construction. Two examples of detailed logs (3261 and 3297) are
69 given.

70
71 **3.3 Field evidence of the eastern landslide**

72 Also the east-facing slope of the same mountain ridge described above, is affected by active deformations (Figs. 9A and
73 10). Here, the Jvari-Khaishi-Mestia road, at an altitude of 715-720 m, is characterized by a series of fractures with two main
74 orientations: one set is parallel to the road, that is to say follows the topographic contour lines with a N-S strike. The other
75 fracture set strikes about E-W, perpendicular to the slope.

76 Most N-S-striking fractures show evidence of extension, with horizontal and vertical offsets of several cm of the road
77 surface. The N-S fractures follow an escarpment that runs along part of this east-facing slope for a total length of about 450
78 m. The height of this scarp is in the order of 3-20 m. At the southern end of the escarpment, the road has deformations with
79 lower amounts of offset. At the foot of the head scarp there is a lake, measuring 43 x 17 m, with the long axis parallel to the
80 local scarp strike (Fig. 10). The lake is associated with local thick clay deposits that require times for their formation. Where
81 the head scarp of the landslide comes closer with the head scarp of the other western landslide, there is the series of long and

Eliminato: 7

Eliminato: 8

Eliminato: 9

Eliminato: i

Eliminato: s

87 wide fissures in the densely-vegetated forest (e.g. Fig. 6D, and Fig. 10). These fissures host several tree trunks whose
88 dimension suggests they are at least some tens of years old.

89 The fractures striking E-W show dominant left-lateral strike-slip motions in the order of several cm of the road surface
90 (e.g. Fig. 9B). A secondary, local extensional (vertical) component is also present. The resulting net slip indicates left-lateral
91 transtensional motions. An old, N-S trending concrete wall, located along the head scarp, is tilted of 5° towards north (Figs.
92 9C-D). It is also left-laterally offset by 190 cm, as measured in November 2015, and 195 cm, as measured in may 2017 (Fig.
93 9E). Nearby, a recent road water channel was also left-laterally offset by 5 cm during a November 2015 measurement (Fig.
94 9F), which increased to 7 cm in may 2017. These offset man-made features are aligned with an offset white strip painted on
95 the asphalt of the Jvari-Khaishi-Mestia road (Fig. 9B). The white strip shows a left-lateral offset of 8 cm. Interviews with local
96 inhabitants and authorities gave indication of an age of AD 1974 for the concrete wall, whereas the white strips were painted
97 two years before we got the offset data.

98 The total area affected by slope deformation is of 0.37 km². In this area, the lacking of drillings did not allow to assess
99 the possible depth of the main slip surface. A simple projection of the possible depth of potential slip surfaces allowed to
00 speculate about a possible range of volume of the total unstable mass of $40 \pm 7 \cdot 10^6$ m³. Anyway, we wish to stress that this
01 estimate must be confirmed by further studies.

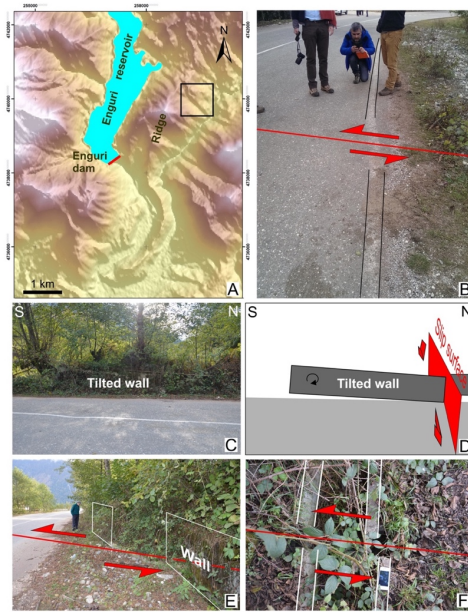
Eliminato: 8

Eliminato: 8

Eliminato: 8

Eliminato: 8

Eliminato: 8



07
08
09
10
11

Figure 9: Features observed at the eastern landslide, located in the box of Figure A. B. Left-lateral offset of the Jvari-Khaishi-Mestia road white strip. C. and D. Photo and interpretation of the tilted wall along the same road. E. Left-lateral offset of 1.9 m of a 1974 AD wall. F. Left-lateral offset of a recent water channel.

Eliminato: 8

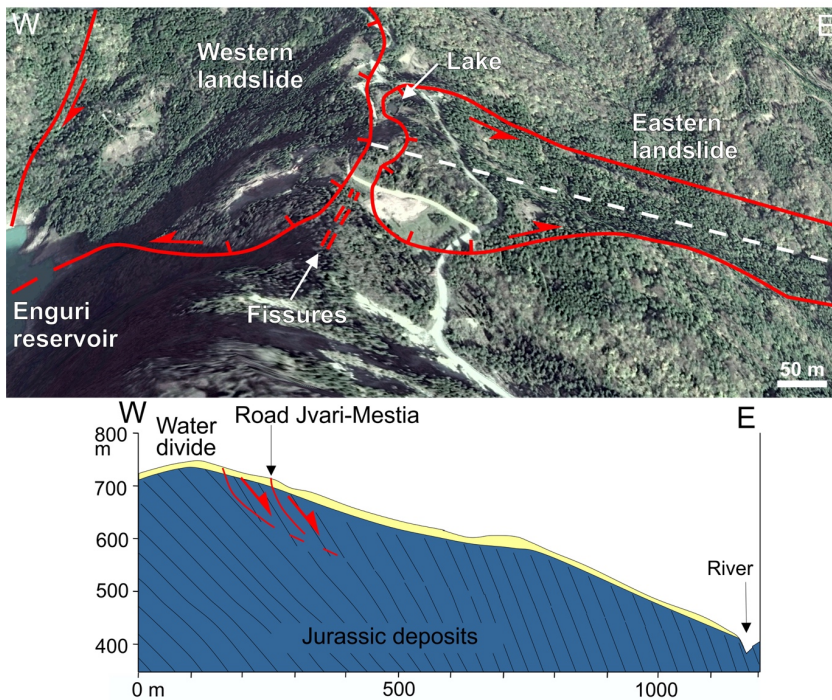


Figure 10: Above: location of the main boundary scarps of the two landslides. Note the small lake at the foot of the head scarp of the eastern landslide, and the fissures located between the head scarps of the two landslides (oblique view from Google Earth). Below: geological section along the eastern landslide, trace is given by the dashed white line in the figure above.

3.4 Slope stability analyses

To assess the stability of the slope, the depth of the possible slip surfaces, the contribution of the water table and its variation, comprising different lake levels, and gauge the impact of possible seismic shaking, we developed a series of analyses of the western landslide; we used the program Slide of Rocscience 7.024, with the approaches of Janbu and Morgenstern-Price, for static conditions, whereas for the seismic stability evaluation, we used the pseudostatic and Newmark modelling.

- Eliminato: 9
- Eliminato: .
- Eliminato: 3.4 Georadar surveys . [1]
- Formattato: Rientro: Prima riga: 0 cm
- Formattato: Tipo di carattere:(Predefinito) Times New Roman, 10 pt, Grassetto
- Formattato: Tipo di carattere:(Predefinito) Times New Roman, 10 pt
- Eliminato: 5
- Eliminato: Numerical modeling
- Eliminato: numerical models
- Eliminato: . For the analyses, we used
- Eliminato: using
- Eliminato: . F

34 The slope stability analyses have been carried out based on the geological/geotechnical model that takes into account
35 data coming from our field surveys, geotechnical tests and logs drilled during the Soviet era (1966) and by CGS (2015). The
36 logs of 1966 are located in the lower slope, between 343 and 546 m a.s.l., in part in correspondence of the area now under the
37 lake level; the more recent logs are located between 566 and 727 m a.s.l. (Fig. 8B). The reconstruction of the stratigraphy of
38 the landslide zone has been done by merging our field surveys with data coming from the logs n. 3291 (done in 1966), located
39 at 403.62 m a.s.l., n. 3297 (1966) at 418.87 m a.s.l., n. 3261 (1966) at 435.62 m a.s.l., and n. BH1, BH3, BH4, BH5 and BH6
40 (done in 2015) located at 570-693.7 m a.s.l., and surveys made by Soviet researchers previous to the dam construction.

Eliminato: 7

41 The present outcropping substrate is made of Jurassic volcano-sedimentary rocks, with interlayering of tuff deposits and
42 sandstones, mostly dipping E to NE (Fig. 8). The same rocks and bedding attitude was surveyed at the foot of the slope before
43 the dam construction. These rocks are locally covered by Quaternary landslide and slope debris deposits. Based on their
44 geotechnical characteristics, the succession has been divided into two geotechnical members: the deepest unit (in brown in
45 Fig. 11) is given by the more intact tuffs and sandstones located below the surface located at a depth between 30 and 80 m.
46 Above this surface, we considered a second geotechnical unit (in green in Fig. 11) made of clay, gypsum, debris and old
47 landslide deposits. Debris contains dominant sandstones and tuff fragmented rocks, with a loam matrix, more rarely a clay
48 matrix, rich in carbonatic and gypsum fragments. Locally, carbonatic fragments dominate. The thickness of this unit is from a
49 few meters to a maximum of 80 m. These two units are covered by late Quaternary deposits that comprise colluvium, eluvium,
50 and shallow debris, with a thickness from 1 to 5 m. These latter, shallow deposits have been incorporated in the geotechnical
51 unit 2 (green unit), due to their low thickness and spatial variability. The geomechanical/geotechnical parameters obtained for
52 the involved materials are presented in Table 1. Considering the high variability of deposits and thus of material properties,
53 we performed a back analysis of the landslide to determine the appropriate material properties.

Eliminato: south

Eliminato: 7

Eliminato: 2

Eliminato: 2

54 Figure 6A locates the piezometric wells that have been used to locate the depth of the water table. Our survey of
55 piezometers showed the presence of water that during May 2017 reached the topographic surface (Table 2). In one well (BH9),
56 the water table showed a temporary artesian behavior. The variation of the Enguri reservoir water level was established based
57 on the information received from the Enguri Dam Company, which indicated the range 430-510 m a.s.l. Taking into account
58 the low hydraulic conductivity of part of the deposits composing the studied slope, the large variations of lake level, and the
59 intense rains that characterize this region, we focused on slope stability analyses that consider the stage of saturation of the
60 involved deposits and did not carry out a transient slope stability analysis. The final material properties used for the modeling
61 were derived based on back analysis and field observations and are presented in bold in Table 1. In particular, the used values
62 of cohesion take into consideration the widespread presence of clastic debris deposits, locally reach in silty clays.

Eliminato: 5

63 In the first static model, the reservoir water level is taken fixed at the maximum level (510 m) (Fig. 11A). The table water
64 level inside the landslide body is assumed as complete saturation as indicated by piezometers during the rainy season. The
65 model indicates that upper parts of the slope are unstable along curvilinear slip surfaces (orange lines) that correspond to Factor
66 of Safety (FS) < 1. Most slip surfaces are shallow (10-30 m) and involve limited parts of the onshore slope.

Eliminato: 2

74 In the second static model, the reservoir water level has been considered at minimum (430 m a.s.l.), resulting in more
 75 diffuse instability of the slope including the part normally below the lake. The relative slip surfaces (orange in Fig. 11B)
 76 correspond to FS < 1, and are mostly deeper (30-80 m) than in the previous case.

Eliminato: 12

77

78 **Table 1.** Geo-mechanical properties of the deposits.

Rock/deposit	Friction angle (ϕ')	Cohesion (c')	Specific weight (γ)	Data source
Clay, measurements in borehole	10-18°	20-47 kPa	19.4-20.1 kN/m ³	(*)
Clay, collected at depth 16-17 m (SH2) and 51-51.2 m (SH4)	16-18°	44-47 kPa	19.2-19.5 kN/m ³	(*)
Weathered bedrock (heavy fractured rock with loam-clay filling)	32°	50 kPa	22 kN/m ³	(x)
Coarse clastic deposit	35-45°	0 kPa	22-23 kN/m ³	(x)
Intact bedrock	35°	200 kPa	25 kN/m ³	(x)
Shallow deposits	16°	0.01-10 kPa	19.65 kN/m ³	(+)
Bedrock	32°	200 kPa	23.5 kN/m ³	(+)

79 (*) Geotechnical Laboratory Tbilisi, (x) field observations and Hoek and Bray, 1981, (+) back analysis and field
 80 observations.

81

82

83 **Table 2.** Location of measured piezometers and water table depth.

Site	Easting (dd.ddd)	Northing (dd.ddd)	Elevation (m asl)	Installed (MM/YY)	Installed depth (m bgs)	Measured depth to water (m bgs)	Measured depth to bottom (m bgs)
BH1	42,049950	42,781550	566,6	07/15	45	7,4	35
BH2	42,050650	42,782500	568,2	07/15	50	1,5	36
BH3	42,049850	42,784583	587	07/15	32	1,3	16
BH4	42,050583	42,784417	652,8	07/15	65	1,3	16
BH5	42,052633	42,787150	679,7	07/15	50	0,0	42
BH5	42,052633	42,787150	679,7	07/15	50	0,5	42
BH6	42,053017	42,779717	725,9	07/15	50	12,0	18
BH7	42,055433	42,781700	721,3	07/15	50	5,8	49
BH8	42,055883	42,786517	704	07/15	55	4,8	23
BH9	42,051800	42,788767	702,6	07/15	51	-0,2	37
BH10	42,051800	42,790167	727,9	07/15	50	Destroyed	Destroyed

84

85

86

88 **Table 3.** Calculated values of PSH.

Vs30	PSH10%	PSH5%	PSH2%	PSH1%	DH_0.5
497	0.45	0.56	0.75	0.91	0.65
548	0.44	0.56	0.74	0.9	0.65
576	0.43	0.56	0.74	0.88	0.65
760	0.4	0.51	0.68	0.82	0.6

89

90 The pseudostatic numerical model was developed using a Peak Ground Acceleration (PGA) that has been selected
91 according to the procedure briefly resumed here below. Since local strong motion records for Georgia do not exist, we selected
92 the seismograph record of Northwestern Balkan Peninsula earthquake (Rep = 19.7 km, depth 3.75 km, Mw = 6.9, Site class
93 B; 1979-04-15, 06:19:41, Lat: 42.04° - Long: 19.05°) (Fig. 12). We have chosen this record from ESM (Engineering Strong-
94 Motion database, <http://esm.mi.ingv.it/>) due to the very similar seismotectonic conditions with respect to the Enguri site and
95 based on probabilistic seismic hazard assessment (PSHA). PSHA was done according to international standards (Sesetyan et
96 al., 2018) based on the reliable catalogue of earthquakes of the region and on the catalogue of active faults of Georgia that
97 provides information on their dimension, strike, dip, kinematics, Mw max, and slip rate, as well as area seismic source zone
98 models (Danciu et al 2018). The ground motion prediction equation model was established for shallow active crustal regions
99 following the criteria by Cotton et al. (2006). For site investigation (estimate Vs30 - average shear velocity for 30 m depth,
00 Table3), we assessed the geophysical characteristics of the deposits affected by the landslide basing on the available borehole
01 data and new measurements by MASW (Multichannel Analysis of Surface Waves) and HVSR (Horizontal to Vertical Spectral
02 Ratio) methods. The MASW approach allowed to assess the relative shear strength of subsurface deposits, which integrated
03 with density values of the local bedrock and overburden sediments (obtained by the logs), resulted in shear modulus (dynamic
04 ground stiffness). We used vertical geophones with 24 channels and 4.5 Hz. The HVSR was based on ambient seismic noise
05 registration “as single measurement”, a method widely used for the site investigation studies in the last two decades (Bard,
06 1999; Bonnefoy-Claudet, 2006). It provides important information on the vertical distribution of P and S seismic wave
07 velocities. In particular, in order to evaluate the S-wave velocity profile with depth, we used the Joint Inversion of Rayleigh
08 wave dispersion curve and H/V curve. This inversion procedure was carried out by a multimodal Monte Carlo inversion based
09 on a modified misfit function (Maraschini and Foti, 2010). We used a Tromino seismometer installed very close to boreholes
10 to compare HVSR curves with local geology and for validation of results. Seismic noise was recorded for 60 minutes at each
11 site, for a total of 13 sites. Measurements were carried out during night or very early morning to avoid any artificial transients.
12 By this way, velocity profiles and Vs30 values were estimated. As an example, the Vp and Vs velocity profiles are shown in
13 Figure 13, where it is possible to appreciate a series of discontinuities that in most cases correspond to the interface with the
14 substratum, or within the Quaternary deposits. In the uppermost part of the landslide, along the Jvari–Mestia road, the Joint
15 Inversion analysis shows relevant resonance interfaces that vary from 14 m to 21 m (from measurement point MST_6 to TR_1

Formattato: Rientro: Prima riga: 1 cm

16 along the road), corresponding to increase of S-wave velocity from 936 m/sec to 985 m/sec. Comparison with log data indicates
17 that this is a discontinuity within the brecciated deposits. The profiles also show another S-wave velocity increase at 51.6 m
18 (MST 9) and 53.6 m (TR 1) corresponding to variation from 1025 m/sec to 1130 m/sec. This might correspond to the interface
19 with the more intact substratum. These measurements, and others corresponding to the lower part of the slope, suggest a
20 geometry of the deposits/rocks corresponding to the geological and geotechnical sections of Figures 8, 11 and 14.

21 In a further step, we prepared a digital elevation model of the slope using topographic maps at a 1:2500 scale. The DEM
22 was converted to a slope map and correlation between slope and Vs30 was adopted for the whole area of the landslide. Finally,
23 taking into account the inputs of source models (the active fault source model and the area source models) and the ground
24 motion prediction equation models, we performed a Probabilistic Seismic Hazard (PSH) assessment in order to individuate
25 the characteristic earthquake for PGA calculation. PSH was calculated for each point taking into account the site characteristic
26 Vs30, for a probability of exceedance of 10%, 5%, 2%, and 1% in 50 years (Table 3). We used the EZFRISK software for
27 earthquake ground motion estimation. Results show that the expected possible scenario is represented by a $PGA = 0.46 g$ for
28 B site class. Finally, the PGA was multiplied by a reference acceleration coefficient of 0.17 (Kavazanjian et al., 1997) to obtain
29 seismic load coefficient = 0.07 ($kh = PGA \times 0.17$).

30 The pseudostatic analysis is presented in (Fig. 14A) with the orange and red slip surfaces corresponding to $FS < 1$.
31 Comparing the static (Fig. 14A) and pseudostatic analysis (Fig. 14A), it is evident that the susceptible slip surfaces are not just
32 restricted to the upper part of the slope but extends all along the Quaternary deposits due to seismic shaking, and are deeper
33 reaching the interface with the substratum. The full dynamic modeling of the slope to estimate the displacements expected
34 from seismic shaking along the slope was done using the Newmark approach. The tolerable displacement is about 1 m
35 (Kavazanjian et al., 1997) and any displacement > 1 m could lead to failure. It is evident from Newmark analysis (Fig. 14B -
36 red slip circles represent failure surfaces that would experience displacements > 1 m) that the whole slope, down to the
37 presently submerged slope toe and even parts of the bedrock, could experience displacements > 1 m. The estimated
38 displacements indicate that the slope is highly susceptible to seismic triggering and could lead to failure of the slope into the
39 reservoir in the event of seismic activity compatible or greater than the PGA here calculated.

40

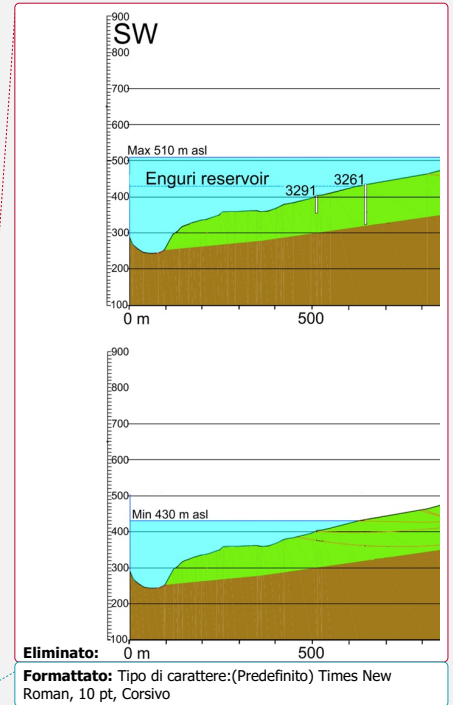
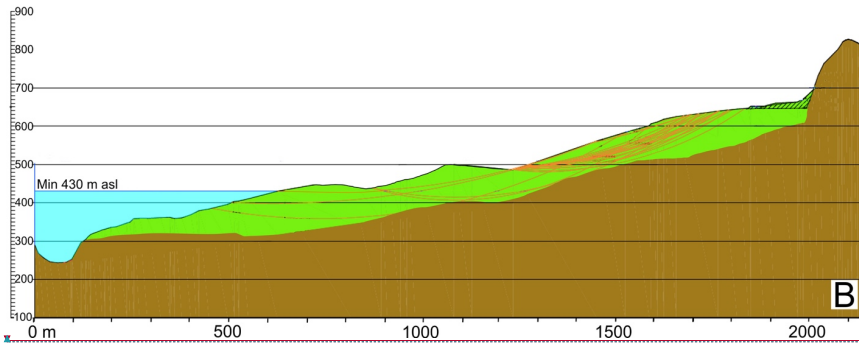
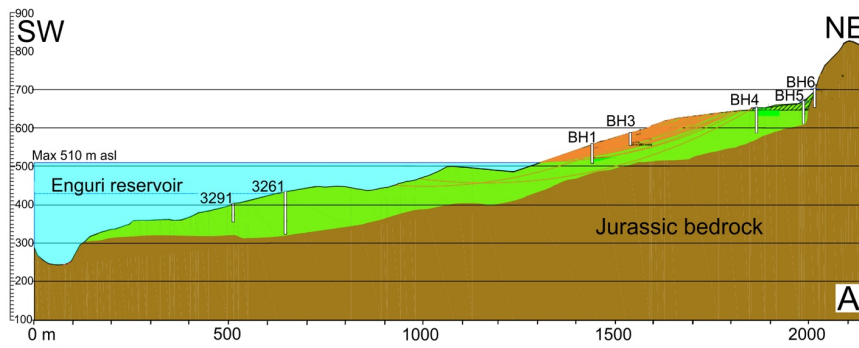
Eliminato: More in detail, the PGA value used in the present study has been appositely determined for the Enguri site, following these steps: we produced models of seismic source zones and their parameterization (estimate recurrence law, maximum magnitude, distribution of earthquakes depth, and nature of movement), using the catalogue of earthquakes that was created for Caucasus and Middle East Region by Zare et al. (2014, 2017) and seismic sources from Danciu et al. (2017). Then we developed appropriate ground motion prediction equation models and seismic hazard curves for spectral amplitudes at each period following the work of Danciu et al. (2016). Site characterisation was carried out based on ambient seismic noise registration "as single measurement" for HVSR (Horizontal to Vertical Spectral Ratio) application and active seismic velocity profiles by using Multichannel Analysis of Surface Waves (MASW). In total, we recorded up to ten ambient seismic noise measurements for the sites where we have also borehole data and performed six active seismic velocity profiles. Altogether site investigation was done for 16 points and Vs30 were estimated. Then, a digital elevation model (DEM) was prepared using topographic maps at a 1:2500 scale. The DEM was converted to a slope map and correlation between slope and Vs30 was adopted for the whole area of the landslide. Finally, Probabilistic Seismic Hazard (PSH) values were calculated for each point taking into account the site characteristics, for a probability of exceedance of 10%, 5%, 2%, and 1% in 50 years (Table 3).

Eliminato: 4

Eliminato: 2

Eliminato: 4

Eliminato: 4

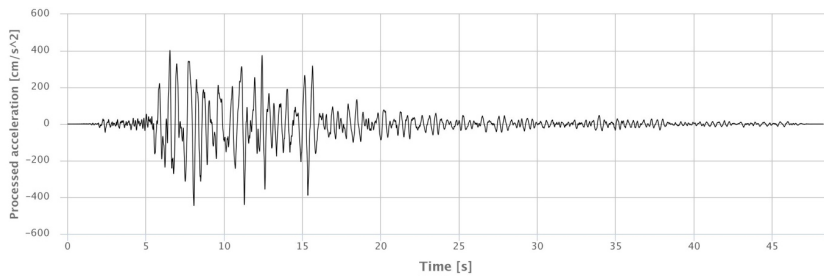


Eliminato:
Formattato: Tipo di carattere:(Predefinito) Times New Roman, 10 pt, Corsivo

- Eliminato:** 2
- Eliminato:** numerical
- Eliminato:** modeling
- Eliminato:** analyze

70
 71
 72 **Figure 11:** Sections of the static analysis developed to assess the effect of variation of the water level in the main
 73 landslide body. A. Instability developed with maximum level of the reservoir water level (orange lines = slip surfaces
 74 with $FS < 1$). B. Analysis of the effect of variation of the reservoir water level down to the minimum level; note new slip
 75 surface (with $FS < 1$) formation at lower elevations.

76

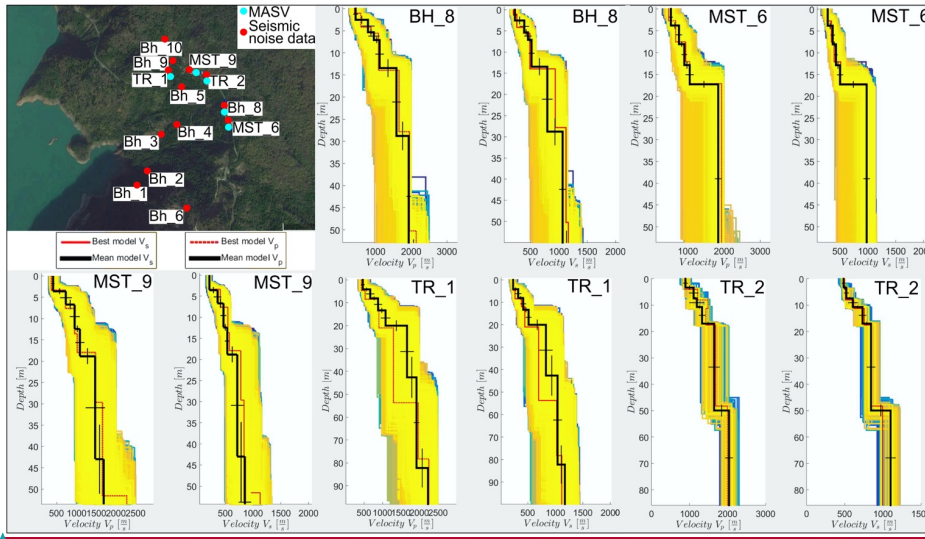


82
83
84
85

Figure 12: Seismic acceleration record used for the pseudostatic and Newmark slope stability analysis. See text for details.

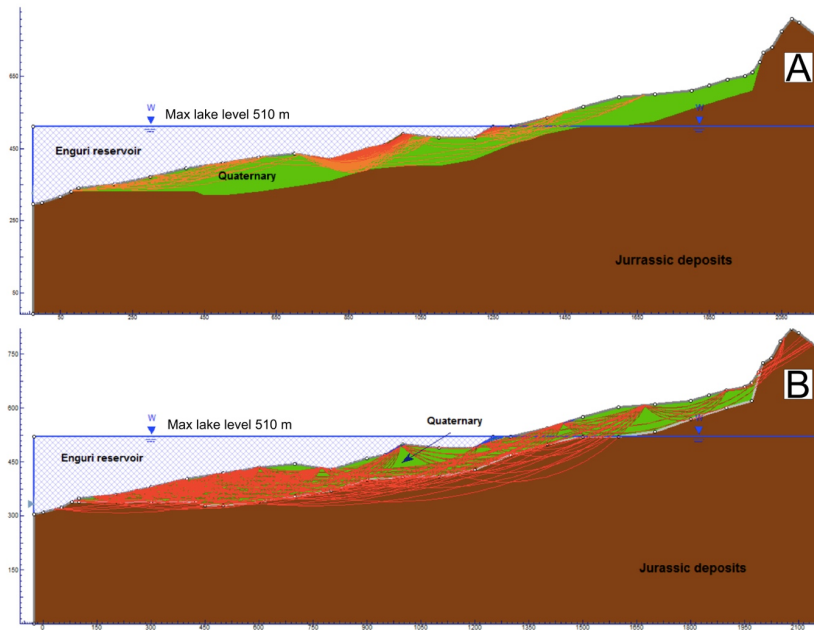
Eliminato: 3

Formattato: Tipo di carattere:(Predefinito) Times New Roman, 10 pt, Grassetto



86
87
88
89

Figure 13. Examples of some of the V_p and V_s velocity profiles measured along the slope affected by the studied western landslide. All sites of MASV and seismic noise measurement are shown in the inset.



91

92 **Figure 14:** Results from seismic slope stability analysis. A. Pseudostatic analysis showing the development of several
 93 potential slip surfaces (orange and red lines) with FS < 1. B. Dynamic modelling, by a Newmark approach, showing the
 94 development of several large slip surfaces (red lines) that would experience more than 1 m of displacement. Since 1 m
 95 is considered critical displacement that would yield to failure, these slip surfaces indicate very unstable conditions along
 96 the slope in case of an earthquake producing the calculated local seismic shaking.

97

98 3.5 Monitoring active deformation

99

100 Due to the evidence of active slope deformation, we installed two digital extensometers (Wire Linear Potentiometric
 101 Transducer, SF500) that record in continuous the deformation across the upper scarp of the western landslide. One
 102 extensometer was installed on 1 November 2016, and the other one a few months later. In Figure 15, we show the data collected
 103 at the older instrument (location at Trench 2, Fig. 7A), together with data regarding lake level variation, amount of rain, and
 104 internal and external (wire) temperatures, from 1 November 2016 to 15 May 2018. The total amount of deformation here is 67
 mm in 18.5 months, which gives an average extension rate of 4.3 cm/y. Deformation largely increased from 16 May 2017 to

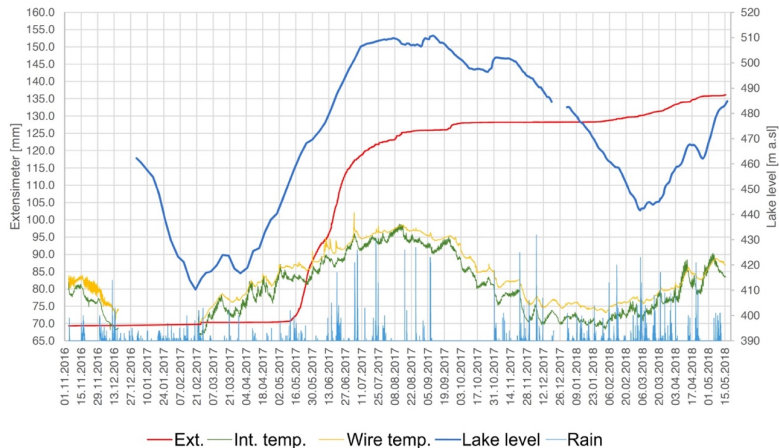
104

Eliminato: 4
 Eliminato: numerical model

Eliminato: 6
 Eliminato: i

Eliminato: i
 Eliminato: 5
 Eliminato: 6

12 8 August 2017 with a total extension of 52 mm that corresponds to a rate of 0.61 mm/day (as a comparison, the average
 13 extension rate is 0.13 mm/day for the whole period of measurement). This interval of extension rate increase follows the almost
 14 complete drawdown of the lake (21 February 2017) and the successive period of lake level infilling, although a delay of about
 15 one month can be recognized. Another interval of rate increase, although much smoother than the previous one, is recognizable
 16 after 6 March 2018, in concomitance with another increase in lake level. During periods of lake level lowering, the extension
 17 here tends to decrease to minimum values. The amount of rain and temperature variations do not seem to affect the extension
 18 values.
 19



— Ext. — Int. temp. — Wire temp. — Lake level — Rain

20
 21 **Figure 15:** Data acquired at one of the two digital extensometers located at the upper scarp of the western landslide
 22 (location Trench 2, Figure 7A). Blue line = lake level, Red line = extension, Yellow line = external (wire) temperature,
 23 Green line = internal temperature, Blue segments = rain amount.

Eliminato: 5
 Eliminato: i
 Eliminato: 6

24
 25 **4 Discussion**

26 **4.1 Evidence of active landsliding**

27 In the study area, we found several evidences of active slope deformation that affect the same mountain ridge on both the
 28 western and eastern flanks. Although part of the western landslide was already locally known as Khoko, this is the first time
 29 that its characteristics are reported in the scientific literature, whereas the eastern landslide has never been recognized before.
 30 For example, in the Geoport of Natural Hazards and Risks in Georgia (<http://drm.cenn.org>), in the section dedicated to

34 landslide hazard, the map reports a medium landslide hazard at all the slopes located east of the Enguri reservoir, without
35 distinction in correspondence of the large, active structures presented in our paper.

36 Regarding the western landslide, the data here presented allowed to define its real total dimension, suggesting that the
37 unstable slope area is larger than the previously known Khoko landslide. We recognized the presence of a main head scarp
38 that runs upward respect to the Jvari-Khaishi-Mestia road (i.e. east of the road, Fig. 6A) in the northern-central part, then
39 crosses the road and runs west of it. This scarp is made of three main segments with the concave side (in plan view) facing
40 west. The segments are interconnected and thus the total head scarp is continuous suggesting that the process of slope instability
41 has already led to link together what originally might have been a series of discrete landslides. Historical and present-day
42 activity along this landslide is manifested by the presence of fissures and slip planes at the foot of the head scarp, subsidiary
43 scarps in the slope, and systematic tilted trees all along the slope. Where the Jvari-Khaishi-Mestia road crosses the active
44 structures, it requires continuous maintenance in order to fill the opening fractures and smooth the scarps created along the
45 slip planes.

46 The eastern landslide shows the main head scarp that runs upward respect to the Jvari-Khaishi-Mestia road (i.e. west of
47 the road, Fig. 10). It is made of a single structure with the concave side (in plan view) facing east. Historical and present-day
48 activity along this landslide is manifested by the presence of fissures along the head scarp, some of which are located in the
49 forest and some cross the Jvari-Khaishi-Mestia road that also here requires continuous maintenance. Moreover, the 1.9 m left-
50 lateral strike-slip offset of the old concrete wall is compatible with landslide movements along the lateral slip plane.

51

52 4.2 An old history of slope deformation

53 We found evidence that the studied western slope has a long history of landsliding. The geological map surveyed during
54 Soviet times, before the infilling of the water reservoir, shows the presence of prehistoric landslide deposits, with a thickness
55 up to 35-40 m, at the lower part of the slope, now submerged (see Fig. 4 and section in Fig. 8B). Moreover, at the foot of the
56 present onshore slope, there are gypsum deposits extremely deformed, which should result from a long history of movements.

57 There are also several evidences suggesting that both the western and eastern landslides have started their movements at least
58 several tens of years ago. The western landslide was already moving during the construction of the pavement of the old Jvari-
59 Khaishi-Mestia road. This road was improved during the construction of the Enguri dam, at the Soviet era, by putting a very
60 thick concrete flooring, as showed in Trench 1 that we opened across one of the active slip planes located at the foot of the
61 head scarp (Fig. 7C). The thickness of 0.5 m of this concrete layer and its presence suggest that it was required possibly due
62 to the recognition at that times of active deformation along this road segment. In fact, during the Soviet era, the general
63 thickness of concrete roads was much lesser. Moreover, the lowered concrete pavement (1.3 m) respect to the present road
64 level, confirms an ongoing process of subsidence here. Then it was followed by the construction of a further road, found 20
65 cm below the present road level in Trench 1 and 2, which also confirms continuous downsagging of the area. Here, the present-
66 day road surface suffers of continuous offsetting with consequent necessity to accumulate further tens of cm of asphalt to
67 maintain the road level.

Eliminato: 5

Eliminato: a

Eliminato: that

Eliminato: 9

Eliminato: The height of the scarp is in the order of 3-20 m, although it is difficult to quantify it precisely due to the local presence of dense vegetation.

Eliminato: an

Eliminato: shows 1.9 m of

Eliminato: left-lateral strike-slip offset

Eliminato: 3

Eliminato: 7

Eliminato: 6

Eliminato: is lowered of

Eliminato: ing

83 Also the eastern landslide has evidence of an old history; the small lake at the foot of the head scarp is here interpreted
84 as resulting from upward tilting of the uppermost part of the landslide body. The thick clay deposits associated to this lake
85 suggest that it has a quite long history. Also the dimension of the trees growth within the fissures located uphill of the head
86 scarp suggests that these fissures opened at least some tens of years ago. Moreover several hand-made structures show
87 incremental offset with age (the concrete wall of the 70' ys, the water channel, the white strips of the asphalt, etc.) confirming
88 the gradual continuous movements of this landslide.

89

90 4.3 Kinematics

91 The height of the head scarp of the western landslide (20-70 m) indicates that the landslide suffered important vertical
92 slip in the head zone. The presence of a wide sub-horizontal to gentle slope at the scarp foot, which has been exploited for the
93 construction of the Jvari-Khaishi-Mestia road, associated with the presence of the head scarp, suggest the development of
94 rotational movements of the upper slope. Ongoing development of vertical scarps in the asphalt of the road, and the presence
95 of gentle scarps in the middle slope, indicate that rotation movements are still present in different zones of the landslide area.
96 The orientation of the active fissures and slip planes surveyed on the road, which are parallel to subparallel to the main head
97 scarp, and the presence of dip-slips along the vertical scarps, indicate a general movement of this western landslide towards
98 the west. In detail, the movement is more complex since the northern part shows motions towards SSW, the central part toward
99 W, and the southern part toward NW. These vectors, together with the general shape of the landslide in plan view, suggest that
00 there is a concentric movement of the landslide body towards the toe zone, where bulging and decrease of motion are expected.
01 Anyway, since the tow zone is under the Enguri lake, it is impossible to verify what occurs in the lowermost part of the
02 landslide.

03 In regard to the eastern landslide, in the field there is clear indication of several meters of vertical slip along the head
04 scarp, at the foot of which there is a flat area that contains the small lake. A portion of this sub-horizontal area has been
05 exploited also here to host the Jvari-Khaishi-Mestia road. These data indicate the presence of rotational movements of the
06 upper slope. The northern lateral boundary of the landslide is characterized by a prolongation of the main head scarp that
07 crosses the road. In this point, there is the 70'-ys-old concrete wall that shows tilting northward compatible with a component
08 of downthrown of the southern block. The same wall also shows the 1.9 left-lateral strike-slip offset that is compatible with
09 the general eastward motion of the landslide body. The northern boundary of the landslide is thus characterized by
10 transtensional movements that also comply with rotational deformation of the upper part of the unstable slope.

11

12 4.4 Slip rates

13 For the western landslide, Trench 1 allows to estimate a long-term (57 ys) slip rate of the vertical component of motion
14 in the order of 2.3 cm/y, based on the age of the oldest buried road made about AD 1960. Our repeated observations on the
15 development of fissures and vertical scarps onto the asphalt of the modern road surface, conducted in the years 2015-2017,
16 indicate slip-rates between < 1 cm/y up to 9 cm/y, depending on the location of the examined structure. We remind that these

Eliminato: first of all, at

Eliminato: there is a lake, measuring 43 x 17 m, with the long axis parallel to the local scarp strike (Fig. 9). The lake is associated with clay deposits that require times for their formation.

Eliminato: Where the head scarp of the landslide comes closer with the head scarp of the other western landslide, there is the series of long and wide fissures in the densely-vegetated forest (e.g. Fig. 5D, and Fig. 9). These fissures host several tree trunks whose dimension

Eliminato: ey are

Eliminato: old

Eliminato: is in the order of

Eliminato: , showing

Eliminato: Dip-slip movements along subvertical planes are confirmed by the GPR survey.

Eliminato: This dip-slip component is confirmed by the GPR surveys, as can be appreciated in the sections of Fig. 10.

Eliminato: Along the southern part of the GPR section of Fig. 10, strata are tilted southward, although the close southward dip of the slip plane visible in the section is compatible with an opposite versus of tilting. We suggest that this strata tilting in reality is connected with the southern lateral boundary of the landslide that is located more southward respect to this GPR section (see Fig. 10A). This boundary is given by a slip plane that here dips to the NE and, as a consequence, should produce tilting of strata towards SW.

41 features are usually destroyed during restoring of the asphalt pavement. The data of the installed extensometer indicate an
42 extension rate of 4.3 cm/y in the last 1.5 years. In general, it seems that the slip rate increases from south to north along the
43 upper part of the landslide, although this observation requires detail measurements to be confirmed. For this reason, we
44 installed a network of 18 bench marks distributed all along the upper part of the landslide. GPS measurements started in the
45 late 2016 and will be published in a future paper.

46 At the eastern landslide, the 190 cm offset of the concrete wall (November 2015) and its age of AD 1974, result in a slip
47 rate of 4.6 cm/y for the long-term (41 ys) motion towards east. The offset measurement in May 2017 of the same wall results
48 in a short-term slip-rate of 3.75 cm/y. The water channel offset was measured between November 2015 and May 2017 giving
49 a short-term slip rate of 1.5 cm/y. The offsets amount and age of the white strips on the road, give estimation of 4 cm/y for the
50 short-term slip rate (2 ys). We remind that also here the road deformation features are destroyed during periodic restoring of
51 the asphalt pavement.

52

53 4.5 Possible origin of slope deformation

54 As regards the dimension and type of the western landslide, for which more data are available, it is necessary to stress
55 that this slope is characterised by the presence of a thick shallow succession of debris and clay-gypsum deposits in the order
56 of at least 30-80 m. This indicates the presence of a thick sequence of deposits that have poor mechanical properties and that
57 are widespread all over the investigated slope. In fact, both static and dynamic analyses indicate the possible development of
58 several slip planes (characterised by $FS < 1$). In particular, the dynamic modelling shows slip surfaces with $FS < 1$ that reach
59 depths in the order of 80–100 m. In the field, there are clear evidence of rotational deformation in the upper part of the unstable
60 slope, accompanied by dip-slip along the planes perpendicular to the general downhill motion. These data do not fit with the
61 interpretation of slope deformation linked to scattered, discrete surficial small landslides, but are instead consistent with a
62 slope affected by a unique landslide. Based on numerical simulations, the depth of the possible slip surfaces that might develop
63 especially under earthquake sollicitation, indicates a probable DSGSD.

64 The similar position and features of the western and eastern landslides cannot be a mere series of coincidences, and we
65 cannot exclude that they have a common origin. The toe of the two unstable slopes are located at 400-300 m a.s.l., which
66 correspond to the level of erosion of the present river located at the foot of the eastern landslide, and to the original river level
67 at the base of the western landslide, now hidden below the Enguri water reservoir. The two river valleys have a *V*-geometry in
68 section view and interest areas mostly at altitudes lower than 1900 m a.s.l., that represents the lower threshold of former
69 glaciers of the Late Glacial Maximum phase (Late Pleistocene) defining the lower boundary of the nival zone (Gobejishvili et
70 al., 2011). This means that the two river valleys might have started to form before the LGM, but they fully developed down to
71 the present depth in consequence of the post-LGM water runoff. Both valleys reach the common flood plain of the Rioni Basin
72 at the same altitude. All these features suggest that the two river valleys developed at the same time, contributing to create the
73 topographic gradient at the two sides of the mountain ridge. Based on all this information, we suggest that the triggering factor

Eliminato: i

Eliminato: same wall's

Eliminato: has been re-

Eliminato: d

Eliminato: showing a total dislocation of 195 cm, and a

Eliminato: ing

Eliminato: the numerical models, both

Eliminato: s,

Eliminato: Finally, our preliminary GPS measurements of bench marks in the upper slope indicate a clear consistent pattern of slope motion and homogenous GPS velocity. All t

85 in the development of the two landslides might have been the increase above a threshold value of the slope dip and of the
86 topographic altitude difference created by river erosion.

87 The formation of the two deep river valleys and the consequent development of the mountain ridge that gave rise to the
88 two landslides, may also be linked with the mountain uplift of the region. An increase in Plio-Pleistocene exhumation rates in
89 northwest Georgia is supported by thermochronometric studies (Vincent et al., 2011) that show the southern flank of the
90 western Greater Caucasus range has undergone rapid exhumation of ~ 1 km/Ma since the Pliocene onwards. In particular, the
91 geological structural setting of the study area is characterized by the presence of thickening of the shallow crustal succession
92 caused by thin-skin tectonics, as introduced in Figure 2. Although the crustal section of Figure 2 is at a much broader scale
93 than the area here studied, it allows to recognize that the landslides developed in a part of the mountain belt subject to enhanced
94 uplift in correspondence of the ramp anticline. Under this structural architecture, and taking into account the seismic activity
95 of western Caucasus (Tsereteli et al., 2016), an earthquake with the consequent ground acceleration cannot be ruled out as
96 possible triggering of one of the two landslides or of both. Landslides aligned along active faults and triggered by seismic
97 activity have been observed frequently elsewhere (e.g. Tibaldi et al., 1995, 2015). Anyway, the available seismic catalogue
98 goes back in the area up to the Tsaishi earthquake of 1614 AD (Tibaldi et al., 2017b), and thus does not allow to establish a
99 possible direct relationship, also in view of the fact that the exact age of inception of these landslides is unknown.

00 A gross estimation of the possible age of the studied landslides can be done if we assume a constant deformation rate;
01 for the western landslide, with the average height of the head scarp (45 m) and average slip rate (3 cm/y), we obtain a rough
02 age of the landslide in the order of 1500 ys. At the eastern landslide, the average height of the head scarp (30 m) and average
03 slip rate (3.5 cm/y), give a gross age estimation in the order of 900 ys.

04 4.6 Hydrogeological hazard

05 Although this is a preliminary description of the evidence and characteristics of the landslides located nearby the Enguri
06 dam, the data here presented are enough to pinpoint a series of relevant results on the hydrogeological hazard of the area. First
07 of all, the western landslide faces directly the Enguri reservoir, with the toe zone of the unstable slope located below the water
08 level, as resulting from the pseudostatic and dynamic analyses that are justified by the fact that the studied area is located in
09 an active tectonic region where earthquakes with Ms up to 7.0 have been recorded (Varazanashvili et al., 2011). This slope
10 moves continuously in a sort of creeping, as already observed elsewhere at DSGSDs (Varnes et al., 1989, 1990, 2000).
11 Anyway, it has been also observed that movements at DSGSDs can be intermittent (Beget, 1985): they can slow down or stop,
12 and then suddenly unrest with rapid downward displacement also in the order of meters, without a complete failure (Tibaldi
13 et al., 2004; Tibaldi and Pasquaré, 2008; Pasquaré Mariotto and Tibaldi, 2016). Anyway, the occurrence of a sudden downhill
14 displacement of the western landslide, for example during seismic shaking as indicated by the Newmark analysis, can involve
15 a huge rock volume, in the order of $48 \pm 12 \cdot 10^6 \text{ m}^3$. This might have effect on the water body, and this hypothesis is worth
16 further studies on the topic.
17

Eliminato: (Fig. 16)

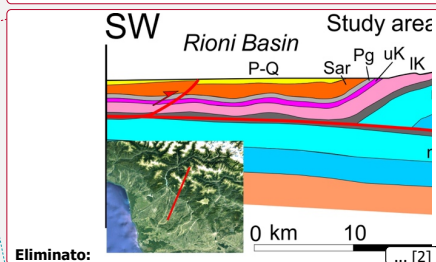
Eliminato: The structural section portrayed in this figure has been obtained by integrating our field surveys with geophysical and geological data from Banks et al. (1997). The section shows the presence of a main basal thrust dipping north. The basal thrust has a ramp-flat geometry that produced a frontal asymmetric ramp anticline. This structure clearly produces local

Eliminato: , exactly where our study area is located (see box in Figure 16)

Eliminato: Moreover, other small reverse faults are located in the area, contributing to further uplift.

Formattato: Rientro: Prima riga: 0,75 cm

Eliminato: .



Eliminato:

Formattato: Tipo di carattere:(Predefinito) Times New Roman, 10 pt, Colore carattere: Nero

Eliminato: numerical

33 Our preliminary static ~~analysis~~ suggests that slope movements can occur both when the lake is at the highest level and
34 when it is lowered. This result does not necessarily suggest a possible catastrophic failure of the slope in static conditions, but
35 is instead coherent with the field evidence of continuous deformation along the slope. We interpret this as a consequence of
36 the characteristics of the deposits along the slope. Slip surfaces can activate especially in the part of the slope above the lake
37 level, because here deposits rich in clays, and very altered tuffs, dominate. When the water table lowers from 510 m to 430 m,
38 although a rapid drawdown condition is created, the shallow deposits of the upper slope remain saturated due to their low
39 hydraulic conductivity. Moreover, increase of movements can occur during phases of saturation of the on-shore landslide body
40 that may take place particularly during the rainy season. At the lowest lake level, slip surfaces can activate in the lower part of
41 the slope due to debuttressing of the slope toe, although the dominance here of deposits with a relatively high hydraulic
42 conductivity.

43 The two studied landslides also pose a threat to other infrastructures like the Jvari-Khaishi-Mestia road, which in fact
44 requires continuous maintenance to avoid the gradual formation of dangerous, tens of decimetres high steps in the asphalt. We
45 highlight also the presence of an inhabited house resting in the middle of the western landslide, and another house recently
46 built close to the northern boundary slip zone of the eastern landslide.

47 In order to contribute to a better assessment of the hydrogeological hazard of the area, we installed two digital
48 extensometers in correspondence of the active head structures of the western landslide, together with the already mentioned
49 bench marks for GPS measurements. This monitoring effort will help to individuate possible alert situations and to better
50 constrain the behaviour of this unstable slope.

51

52 **4.7 Comparison with other landslides**

53 Here we focus on the western landslide, its relations with the artificial lake, and similar settings reported by literature.
54 As shown by the Quaternary geological deposits and by the presence of the high head scarp, the studied area was already
55 interested by the emplacement of landslide deposits in prehistoric times. The already destabilized slope was thus interested by
56 the formation of the Enguri reservoir and its level variations. The creation of artificial lakes can have different effects: on one
57 side, it triggers possible seepage process resulting in an increase in pore water pressure within the slope deposits, thus reducing
58 their shear strength. On the other side, the presence of the lake water body induces a stabilizing load at the toe of the submerged
59 part of the slope (Paronuzzi et al., 2013). In transient conditions, the rate of lake filling or drawdown, combined with the
60 permeability of the bank-forming materials, produce different effects of reservoir level changes. Several landslides, in fact,
61 have been triggered by filling–drawdown operations (Schuster, 1979; Kenney, 1992; Zhu et al., 2011), as well as pre-existing,
62 ancient landslides have been reactivated during water reservoir formation (e.g. Kaczmarek et al., 2015).

63 In the case of low permeability of slope materials, rapid drawdown of the lake level can produce a decrease in the factor
64 of safety, possibly leading to slope failure (Kenney, 1992). A rapid decrease in lake level, in fact, results in a short-term
65 increase in hydraulic gradient in adjacent slopes (Jones et al., 1961; Schuster and Wiczorek, 2002; Deying et al., 2010; Pinyol
66 et al., 2012). For example, in Japan about 60% of reservoir landslides occurred during sudden decrease of the water level

Eliminato: numerical modelling

Eliminato: i

69 (Nakamura, 1990). At a DSGSD located above the Gepatsch dam reservoir (Austrian Alps), slope deformation rates correlate
70 with reservoir levels and drawdown conditions (Zangerl et al., 2010). In the case, instead, of high permeability of bank-forming
71 materials, the reservoir level increase can produce a decrease in the factor of safety. For example, at the Vajont (Italy)
72 catastrophic landslide, detailed numerical analyses by Paronuzzi et al. (2013) show the predominant role played by reservoir
73 levels in determining slope instability, respect to the rain-induced water table in the upper slope. In particular, the initial large
74 slope deformation took place in concomitance with the lake level rise. Consistent with this trend, the final collapse of 9 October
75 1963 coincided with the maximum reservoir level reached. Paronuzzi et al. (2013) also show that the decisive geological factor
76 contributing to the Vajont collapse was the presence of an already existing landslide: the prehistoric rockslide was
77 characterized by materials with high permeability and a thick shear zone at the base, including montmorillonitic clay lenses.
78 The combination of poor mechanical properties of clay beds with the high permeability of the angular limestone gravel,
79 determined a rapid reservoir-induced inflow that reduced strength and factor of safety. A further example is given by the
80 Byford Creek slide, located above the Clyde Dam reservoir (New Zealand). Here, long-term creep movements show a clear
81 reaction to lake filling, with a first large increase in the deformation rate and long-term slowing of movement (Macfarlane,
82 2009).

83 The landslide here studied, at distance of more than 40 years from the construction of the Enguri reservoir, still shows a
84 high sensitivity to water infilling operations. The unstable slope behavior, during large water level variations, is similar to
85 other landslides with bank-slope material characterized by high permeability. In particular, the deposits found in the logs of
86 the lower part of the slope (below about 500 m a.s.l.), being characterized by the dominance of angular carbonatic clasts with
87 interspersed clays, recall those present at other landslides where the factor of safety decreases with increase of lake level. With
88 such characteristics of the involved materials, during reservoir increase the pore water pressure effect on the shear strength
89 prevails over the stabilizing buttressing of the lake water body, inducing an acceleration in slope movements. This is testified
90 by the acceleration in slope deformation following the Enguri reservoir infilling (Fig. 15).

91

92 **5 Conclusions**

93 We presented for the first time the evidence and characteristics of two large landslides located nearby the Enguri dam
94 and water reservoir, in the southwestern part of the Caucasus (Republic of Georgia).

95 The landslides affect the two opposite slopes of a mountain ridge that runs parallel to the Enguri reservoir. The slope
96 directly facing the reservoir shows active deformations that involve a subaerial area of 1.2 km². Field data, information coming
97 from wells, seismological data with calculation of the local Peak Ground Acceleration (PGA), and slope stability analyses,
98 indicate different depths of the possible sliding surfaces depending on various parameters. The worst scenario is given by the
99 occurrence of a PGA compatible with the highest seismicity of the region, which can contribute to activate slip surfaces at
00 depths corresponding to a volume of the unstable mass up to $48 \pm 12 \cdot 10^6 \text{ m}^3$.

01 The head scarp zones of both landslides interest the main Jvari-Khaishi-Mestia road with offsets of man-made features
02 that indicate short-term (last 2 years) slip rates up to 9.3 cm/y and long-term (last 55 years) slip rates up to 4.6 cm/y.

Eliminato: 5

Eliminato: Ground Penetrating Radar surveys,

Eliminato: numerical modelling

06 The possible causes for the past inception of the two landslides can be multiple. First of all, we propose the increase
07 above a threshold value of the slope dip and of the topographic altitude difference created by river erosion. The toe zones of
08 both landslides, in fact, are located in correspondence of deeply entrenched rivers; the river's location at the foot of the western
09 landslide is now below the Enguri water reservoir. The excavation of the two parallel river valleys, in turn, can be linked with
10 the increase in Plio-Pleistocene exhumation rates of this mountain area of ~ 1 km/Ma. The study area, in particular, is located
11 above an anticlinal fold linked with a ramp thrust fault. A tectonic seismic mechanism, with the consequent ground
12 acceleration, cannot be ruled out as possible triggering of one of the two landslides or of both.

13 Extensometer measurements across the head scarp of the western landslide, indicate a present-day variable deformation
14 (average 4.3 cm/y). The deformation rate variations are poorly consistent with rain amount, whereas extensometer data suggest
15 that the landslide body is more sensitive to reservoir filling operation, in consequence of the geotechnical characteristics of the
16 bank-slope materials. During large lake level decrease, the low hydraulic conductivity of the upper slope may contribute to
17 increase movements in the onshore part of the slope. During large lake level increase, the higher permeability of the deposits
18 of the lower slope, mostly constituted by ancient landslide deposits and slope debris, may facilitate acceleration in slope
19 motion.

20

21 **Competing interests**

22 The authors declare that they have no conflict of interest.

23

24 **Acknowledgments**

25 We acknowledge an anonymous referee for his useful suggestions on a previous version of the paper. This study has been
26 conducted in the framework of the NATO project SFP G4934 "Georgia Hydropower Security", of the International Lithosphere
27 Program - Task Force II, of the European Space Agency project n. 32309 "Active tectonics and seismic hazard of southwest
28 Caucasus by remotely-sensed and seismological data" (Leader A. Tibaldi), and of project 216758 of the Shota Rustaveli
29 National Science Foundation.

30

31 **References**

32 Adamia, Sh., Lordkipanidze, M. B., and Zakariadze, G. S.: Evolution of an active continental margins exemplified by the
33 alpine history of the Caucasus, *Tectonophysics*, 40, 183-199, 1977.

34 Adamia, Sh., Alania, V., Chabukiani, A., Chichua, G., Enukidze, O., and Sadradze, N.: Evolution of the Late Cenozoic basins
35 of Georgia (SW Caucasus): a review, In: *Sedimentary basin tectonics from the Black Sea and Caucasus to the Arabian Platform*
36 (eds. M. Sosson, N. Kaymakçı, R. Stephenson, F. Bergerat), Geological Society, London, Special Publication, 340, 239-259,
37 2010.

Eliminato: i

Eliminato: i

40 Adamia, Sh., Alania, V., Tsereteli, N., Varazanashvili, O., Sadradze, N., Lursmanashvili, N., and Gventsadze, A.: Post-
41 Collisional Tectonics and Seismicity of Georgia. In: Tectonic Evolution and Seismicity of south-west Asia. Geological Society
42 of America (GSA) Special Paper (in press), 2017.

43 Adamia, Sh., Zakariadze, G., Chkhotua, T., Chabukiani, A., Sadradze, N., Tsereteli, N., and Gventsadze, A.: Geology of the
44 Caucasus: A Review, Turkish Journal of Earth Sciences, 20, 489–544, 2011.

45 [Alania, V., Chabukiani, A., Chagelishvili, R., Enukidze, O., Gogrichiani, K., Razmadze, A., and Tsereteli, N.: Growth](#)
46 [structures, piggyback basins and growth strata of Georgian part of Kura foreland fold and thrust belt: implication for Late](#)
47 [Alpine kinematic evolution. In Tectonic Evolution of the Eastern Black Sea and Caucasus \(eds M. Sosson, R. Stephenson &](#)
48 [Sh. Adamia\), Geological Society of London, Special Publications, 428, doi:10.1144/SP428.5, 2016.](#)

49 Avagyan A., Sosson, M., Karakhanian, A., Philip, H., Rebai, S., Rolland, Y., Melkonyan, R., and Davtyan, V.: Recent tectonic
50 stress evolution in the Lesser Caucasus and adjacent regions, In. Sosson, M., Kaymakci, N., Stephenson, R. A., Bergerat, F.
51 & Starostenko, V. (eds), Sedimentary Basin Tectonics from the Black Sea and Caucasus to the Arabian Platform. Geological
52 Society, London, Special Publications, 340, 393–408, DOI: 10.1144/SP340.17 0305-8719/10, 2010.

53 Avdeev, B., and Niemi N. A.: Rapid Pliocene exhumation of the central Greater Caucasus constrained by low-temperature
54 thermochronometry, Tectonics, 30, TC2009, doi:10.1029/2010TC002808, 2011.

55 Banks, C., Robinson, A., and Williams, M.: Structure and regional tectonics of the Achara-Trialeti fold belt and the adjacent
56 Rioni and Kartli foreland basins. Republic of Georgia, In Regional and Petroleum geology of the Black Sea and Surrounding
57 Region (ed. A. G. Robinson), American Association of Petroleum Geologists Memoir no. 68, 331-336, 1997.

58 [Bard, P.-Y.: Microtremor measurements: a tool for site effect estimation. In: Irikura, K., Kudo, K., Okada, H., Sasatani, T.](#)
59 [\(Eds\), The effects of surface geology on seismic motion. Balkema, Rotterdam, 1251–1279, 1999.](#)

60 Barrier, E., and Vrielynck, B.: Palaeotectonic Map of the Middle East, Atlas of 14 Maps, Tectonosedimentary-palinspastic
61 Maps from Late Norian to Pliocene, Commission for the Geological Map of the World, Paris, 2008.

62 Bazzurro, P., and Cornell, C. A.: Deaggregation of seismic hazard, Bull. Seism. Soc. Am., 89, 501–520, 1999.

63 Beck, A.C.: Gravity faulting as a mechanism of topographic adjustment, New Zealand Journal of Geology and Geophysics,
64 11, 191–199, 1968.

65 Beget, J.E.: Tephrochronology of antislope scarps on an alpine ridge near Glacier Peak, Washington, U.S.A. Arctic and Alpine
66 Research, 17, 143-152, 1985.

67 [Bonney-Claudet, S., Cotton, F., Bard, P.-Y., Cornou, C., Ohrnberger, M., and Wathelet, M.: Robustness of the H/V ratio](#)
68 [peak frequency to estimate 1D resonance frequency, in: Proceedings of the 3rd International Symposium on the Effects of](#)
69 [Surface Geology on Seismic Motion, 2006.](#)

Formattato: Inglese (Stati Uniti)

70 [CGS \(Center Geodynamic Studies L.L.C.\): Implementation of a complex engineering-geological survey of the left bank of the](#)
71 [landslide in the reservoir area of arch dam LLC «Enguri HPP» and slope stability analysis, Technical report, Moscow, 2015.](#)

72 Chigira, M., and Kiho, K.: Deep-seated rockslide avalanches preceded by mass rock creep of sedimentary rocks in Akaishi
73 Mountains, central Japan, *Engineering Geology*, 38, 221-230, 1994.

74 [Cotton, F., Scherbaum, F., Bommer, J.J., Bungum, H.: Criteria for selecting and adjusting ground-motion models for specific](#)
75 [target applications: applications to Central Europe and rock sites, *J. Seismol.*, 10\(2\), 137–156, 2006.](#)

76 Danciu, L., Kale, O., and Akkar, S.: The 2014 earthquake model of the Middle East: ground motion model and uncertainties,
77 *Bull. Earthquake Engineering*, 1-37, 2016.

78 Danciu, L., Şeşetyan, K., Demircioglu, M., Gülen, L., Zare, M., Basili, R., Elias, A., Adamia, S., Tsereteli, N., Yalçın, H., Asif
79 Khan, M.U.M., Saya, M., Hessami, K., Rovida, A., Stucchi, M., Burg, J.-P., Karakhanian, A., Babayan, H., Avanesyan, M.,
80 Amadli, T., Al-Qaryouti, M., Kalafat, D., Varazanashvili, O., and Erdik, M.: The 2014 earthquake model of the Middle East:
81 seismogenic sources, *Bulletin of Earthquake Engineering*, 1-32, DOI: 10.1007/s10518-017-0096-8, 2018.

82 Deying, L., Kunlong, Y., and Chin, L.: Analysis of Baishuihe landslide influenced by the effects of reservoir water and rainfall,
83 *Environ. Earth Sci.*, 60, 677–687, doi:10.1007/s12665-009-0206-2, 2010.

84 Evans, S.G., and Couture, R.: The 1965 Hope Slide, British Columbia; catastrophic failure of a sagging rock slope, *Abstracts*
85 *with Programs-Geological Society of America*, 16-26, 2002.

86 Forte, A., Cowgill, E., Bernardin, T., Kreylos, O., and Hamann, B.: Late Cenozoic deformation of Kura fold-thrust belt,
87 southern Greater Caucasus, *Geological Society of American Bulletin*, 122, 465-86, 2010.

88 Gobejshvili, R., Lomidze, N., and Tielidze, L.: Late Pleistocene (Würmian) Glaciations of the Caucasus, In J. Ehlers, P.L.
89 Gibbard and P.D. Hughes, editors: *Developments in Quaternary Science*, 15, 141-147, ISBN: 978-0-444-53447-7, 2011.

90 Gutiérrez-Santolalla, F., Acosta, E., Rios, S., Guerrero, J., and Lucha, P.: Geomorphology and geochronology of sackung
91 features (uphill-facing scarps) in the Central Spanish Pyrenees, *Geomorphology*, 69, 298-314, 2005.

92 Hoek, E., and Bray, J.W.: *Rock Slope Engineering*, Revised third edition, The Institution and Metallurgy of Mining, London,
93 1981.

94 Jones, F.O., Embody, D.R., and Peterson, W.L.: Landslides along the Columbia River Valley, Northeastern Washington, US
95 Geological Survey Professional Paper, 367, 1961.

96 Kaczmarek, H., Tyszkowski, S., and Banach, M.: Landslide development at the shores of a dam reservoir (Włocławek, Poland),
97 based on 40 years of research, *Environmental Earth Sciences*, 74(5), 4247-4259, 2015.

Eliminato: .

Eliminato: 7

00 Kavazanjian, Jr, E., Matasovic, N., Hadj-Hamou, T., and Sabatini, P. J.: Geotechnical Engineering Circular No. 3: Design
01 Guidance, Geotechnical Earthquake Engineering for Highways. Volume I-Design Principles (No. Report No: FHWA-SA-97-
02 076), 1997.

03 Kenney, T.C.: Slope stability in artificial reservoirs: influence of reservoir level, selected cases, and possible solutions, In:
04 Semenza, E., Melidoro, G. (Eds.), Proceedings of the meeting on the 1963 Vajont landslide, 17-19 September 1986, Ferrara,
05 Consiglio and Vajont. Grafica Ferrarese, Ferrara, Italy, 67-85, 1992.

06 Koçyiğit, A., Yılmaz, A., Adamia, S., and Kuloshvili, S.: Neotectonics of East Anatolia Plateau (Turkey) and Lesser Caucasus:
07 Implication for transition from thrusting to strike-slip faulting, *Geodinamica Acta*, 14,177-195, 2001.

08 Macfarlane, D.F.: Observations and predictions of the behaviour of large, slow-moving landslides in schist, Clyde Dam
09 reservoir, New Zealand, *Engineering Geology*, 109(1-2), 5-15, 2009.

10 Mahr, T.: Deep-reaching gravitational deformations of high mountain slopes, *Bulletin of the International Association of*
11 *Engineering Geology*, 16, 121-127, 1977.

12 [Maraschini, M., and Foti, S.: A Monte Carlo multimodal inversion of surface waves. *Geophysical Journal International*, 182\(3\),
13 1557-1566, 2010.](#)

14 McCalpin, J.: Criteria for determining the seismic significance of sackungen and other scarplike landforms in mountainous
15 regions. *Techniques for Identifying Faults and Determining their Origins*, U.S. Nuclear Regulatory Commission, Washington,
16 255–259, 1999.

17 McCalpin, J.P., and Irvine, J.R.: Sackungen at the Aspen Highlands ski area, Pitkin County, Colorado, *Environmental and*
18 *Engineering Geoscience*, 1, 277-290, 1995.

19 McGuire, R. K.: Computations of Seismic Hazard, *Annali di Geofisica*, 36, 181-200, 1995.

20 Meijers, M.J., Smith, B., Kirscher, U., Mensink, M., Sosson, M., Rolland, Y., Grigoryan, A., Sahakyan, L., Avagyan, A.,
21 Langereis, C., and Müller, C.: A paleolatitude reconstruction of the South Armenian Block (Lesser Caucasus) for the Late
22 Cretaceous: Constraints on the Tethyan realm, *Tectonophysics* 644, 197–219, 2015.

23 Mosar, J., Kangarli, T., Bochud, M., Glasmacher, U. A., Rast, A., Brunet, M., Sosson, M.: Cenozoic–Recent tectonics and
24 uplift in the Greater Caucasus: a perspective from Azerbaijan, In: *Sedimentary basin tectonics from the Black Sea and*
25 *Caucasus to the Arabian Platform* (eds. M. Sosson, N. Kaymakçı, R. Stephenson, F. Bergerat), Geological Society, London,
26 Special Publication, 340, 261–279, 2010.

27 Nakamura, K.: On reservoir landslide, *Bulletin on Soil and Water Conservation*, (In Chinese), 10(1), 53-64, 1990.

28 Paronuzzi, P., Rigo, E., and Bolla, A.: Influence of filling–drawdown cycles of the Vajont reservoir on Mt. Toc slope stability,
29 *Geomorphology*, 191, 75-93, 2013.

Formattato: Inglese (Stati Uniti)

Formattato: Inglese (Stati Uniti)

Formattato: Inglese (Stati Uniti)

30 Pasquarè Mariotto, F. A., and Tibaldi, A.: Inversion kinematics at deep-seated gravity slope deformations revealed by
31 trenching techniques, *Nat. Hazards Earth Syst. Sci.*, 16, 663-674, 2016.

32 Pasquarè, F.A., Tormey, D., Vezzoli, L., Okrostsvardize, A., and Tutberidze, B.: Mitigating the consequences of extreme
33 events on strategic facilities: Evaluation of volcanic and seismic risk affecting the Caspian oil and gas pipelines in the Republic
34 of Georgia, *Journal of Environmental Management*, 92, 1774-1782, 2011.

35 Pasuto, A., and Soldati, M.: Rock spreading. In: Dikau, R., Brunsten, D., Schrott, L., Visen, M.-L. (Eds.), *Landslide*
36 *recognition, Identification, movement and causes.* Wiley, Chichester, 122-136, 1996.

37 Pinyol, N., Alonso, E., Corominas, J., and Moya J.: Canelles landslide: modelling rapid drawdown and fast potential sliding,
38 *Landslides*, 9, 33–51, doi:10.1007/s10346-011-0264-x, 2012.

39 Radbruch-Hall, D.H.: Gravitational creep of rock masses on slopes, In: Voight, B. (Ed.), *Rockslides and Avalanches*, 1, *Natural*
40 *Phenomena, Developments in Geotechnical Engineering*, 14A, 607-657, 1978.

41 Rebai, S., Philip, H., Dorbath, L., Borissoff, B., Haessler, H. and Cisternas, A.: Active tectonics in the Lesser Caucasus:
42 coexistence of compressive and extensional structures, *Tectonics*, 12 (5), 1089–1114, 1993.

43 Reilinger, R.E., McClusky, S.C., Oral, M.B., King, R.W., Toksoz, M.N., Barka, A.A., Kinik, I., Lenk, O., and Sanli, I.: Global
44 Positioning System measurements of present-day crustal movements in the Arabia-Africa-Eurasia plate collision zone, *Journal*
45 *of Geophysical Research*, 102 (5), 9983–9999, 1997.

46 Reilinger, R.E., McClusky, S.C., Vernant, P., Lawrence, S., Ergintav, S., Cakmak, R., Ozener, H., Kadirov, F., Guliev, I.,
47 Stepanian, R., Nadariya, M., Hahubia, G., Mahmoud, S., Sakr, K., Arrajehi, A., Paradissis, D., Al-Aydrus, A., Prilepin, M.,
48 Guseva, T., Evren, E., Dmirotsa, A., Filikov, S. V., Gomez, F., Al-Ghazzi, R., and Karam, G.: GPS constraints on continental
49 deformation in the Africa-Arabia-Eurasia continental collision zone and implications for the dynamics of plate interactions,
50 *Journal of Geophysical Research*, 111(B5), doi: 10.1029/2005JB004051, 2006.

51 Schuster, R.L.: Reservoir-induced landslides, *Bulletin of the International Association of Engineering Geology*, 20, 8-15, 1979.

52 Schuster, R.L., and Wieczorek, G.F.: Landslide triggers and types, In: Rybar J., Stemberk J., Wagner P. (eds), *Proc. 1st*
53 *European Conference on Landslides*, Prague, Czech Republic, Balkema Publishers, Taylor & Francis, Prague, 59–78, 2002.

54 [Şeşetyan, K., Danciu, L., Demircioğlu Tümsa, M.B., Giardini, D., Erdik, M., Akkar, S., M. Gülen, L., Zare, M., Adamia, S.,](#)
55 [Ansari, A., Arakelyan, A., Askan, A., Avanesyan, M., Babayan, H., Chelidze, T., Durgaryan, R., Elias, A., Hamzehloo, H.,](#)
56 [Hessami, K., Kalafat, D., Kale, O., Karakhanyan, A., Asif Khan, M., Mammadli, T., Al-Qaryouti, M., Sayab, M., Tsereteli,](#)
57 [N., Utkucu, M., Varazanashvili, O., Waseem, M., Yalçın, H., Tolga Yılmaz, M.: The 2014 seismic hazard model of the Middle](#)
58 [East: overview and results. *Bulletin of Earthquake Engineering*, 1-32, 2018.](#)

Formattato: Inglese (Stati Uniti)

59 Semenza, E., and Ghirotti, M.: History of the 1963 Vaiont slide: the importance of geological factors, *Bulletin of Engineering*
60 *Geology and the Environment*, 59(2), 87-97, 2000.

61 Solonenko, V.P.: Landslides and collapses in seismic zones and their prediction, *Bulletin of the International Association of*
62 *Engineering Geology* 15, 4–8, 1977.

63 Sosson, M., Rolland, Y., Danelian, T., Muller, C., Melkonyan, R., Adamia, S., Kangarli, T., Avagyan, A., and Galoyan, G.:
64 Subductions, obduction and collision in the Lesser Caucasus (Armenia Azerbaijan, Georgia), new insights, In: Sosson, M.,
65 Kaymakci, N., Stephanson, R., Bergarat, F., Storatchenoko, V. (Eds.), *Sedimentary Basin Tectonics from the Black Sea and*
66 *Caucasus to the Arabian Platform*, Geological Society of London Special Publication, 340, 329–352, 2010.

67 Tan, O., and Taymaz, T.: Active tectonic of the Caucasus: earthquake source mechanisms and rupture histories obtained from
68 inversion of teleseismic body waves, *Geological Society of America*, special paper 409, 531-578, 2006.

69 Tibaldi, A., and Pasquarè, F.: Quaternary deformations along the ‘Engadine–Gruf tectonic system’, Swiss–Italian border,
70 *Journal of Quaternary Science*, 23(5) 475–487, 2008.

71 Tibaldi, A., and Tsereteli, N.: International effort tackles landslide hazards to keep the peace, *Eos*, 98,
72 doi:10.1029/2017EO065815. Published on 30 January 2017.

73 Tibaldi, A., Ferrari, L., and Pasquarè, G.: Landslides triggered by earthquakes and their relationships with faults and mountain
74 slope geometry: an example from Ecuador, *Geomorphology*, 11, 215-226, 1995.

75 Tibaldi, A., Rovida, A., and Corazzato C.: A giant deep-seated slope deformation in the Italian Alps studied by
76 paleoseismological and morphometric techniques, *Geomorphology*, 58, 27–47, 2004.

77 Tibaldi, A., Corazzato, C., Rust, D., Bonali, F. L., Mariotto, F. P., Korzhenkov, A. M., Oppizzi P., and Bonzanigo, L.: Tectonic
78 and gravity-induced deformation along the active Talas–Fergana Fault, Tien Shan, Kyrgyzstan, *Tectonophysics*, 657, 38-62,
79 2015.

80 Tibaldi, A., Alania, V., Bonali, F. L., Enukidze, O., Tsereteli, N., Kvavadze, N., and Varazanashvili, O.: Active inversion
81 tectonics, simple shear folding and back-thrusting at Rioni Basin, Georgia, *Journal of Structural Geology*, 96, 35-53, 2017a.

82 Tibaldi, A., Russo, E., Bonali, F.L., Alania, V., Chabukiani, A., Enukidze, O., and Tsereteli, N.: 3-D anatomy of an active
83 fault-propagation fold: a multidisciplinary case study from Tsaishi (Georgia), western Caucasus, *Tectonophysics*, 717, 253-
84 269, 2017b.

85 Tsereteli, N., Tibaldi, A., Alania, V., Gventsadse, A., Enukidze, O., Varazanashvili, O., and Müller B.I.R.: Active tectonics of
86 central-western Caucasus, Georgia, *Tectonophysics*, 691, B, 328-344, 2016.

87 Varazanashvili, O., Tsereteli, N., Bonali, F. L., Arabidze, V., Russo, E., Pasquarè Mariotto, F., Gogoladze, Z., Tibaldi, A.,
88 Kvavadze, N., and Oppizzi, P.: GeoInt: the first macroseismic intensity database for the Republic of Georgia, *Journal of*
89 *Seismology*, 1-43, doi.org/10.1007/s10950-017-9726-5, 2018.

90 Varnes, D.J., Coe, J.A., Godt, J.W., Savage, W.Z., and Savage, J.E.: Measurement of ridge-spreading movements (sackungen)
91 at Bald Eagle Mountain, Lake County, Colorado, II: continuation of the 1975–1989 measurements using a Global Positioning
92 System in 1997 and 1999, U.S. Geological Survey, Open file report 00-205, on-line edition, 2000.

93 Varnes, D.J., Radbruch-Hall, D.H., and Savage, W.Z.: Topographic and structural conditions in areas of gravitational
94 spreading of ridges in the western United States, U.S. Geological Survey Professional Paper, 1496, 28 pp, 1989.

95 Varnes, D.J., Radbruch-Hall, D.H., and Varnes, K.L.: Measurement of ridge spreading movements (sackungen) at Bald Eagle
96 Mountain, Lake County, Colorado, 1975–1989, U.S. Geological Survey, Open File Report, 90-543, 13 pp, 1990.

97 Vincent, S.J., A. Carter, V.A. Lavrishchev, S.P. Price, T.G. Barabadze, and Hovius N.: The exhumation of the western Greater
98 Caucasus: a thermochronometric study, *Geological Magazine*, 148, 1–21, 2011.

99 Vincent, S.J., Morton, A.C., Carter, A., Gibbs, S., and Teimuraz, G.B.: Oligocene uplift of the Western Greater Caucasus: An
00 effect of initial Arabia-Eurasia collision, *Terra Nova*, 19, 160–166, 2007.

01 Zangerl, C., Eberhardt, E., and Perzmaier, S.: Kinematic behaviour and velocity characteristics of a complex deep-seated
02 crystalline rockslide system in relation to its interaction with a dam reservoir, *Engineering Geology*, 112, 53-67, 2010.

03 ~~Zolotarev, G.S., Makhorin, A.A., and Federenko, V.S.: Geological map of left bank of river Enguri, upper part of Enguri HPP,~~
04 ~~Scale 1:2500, Ministry of Energy, CCCP, 1968.~~

05 Zhu, D., Yan, E., Hu, G., and Lin, Y.: Revival deformation mechanism of Hefeng Landslide in the Three Gorges Reservoir
06 based on FLAC3D software, *Procedia Engineering*, 15, 2847-2851, 2011.

07

Eliminato: Zare, M., Amini, H., Yazdi, P., Sesetyan, K., Demircioglu, M.B., Kalafat, D., Erdik, M., Giardini, D., Khan, M.A., and Tsereteli N.: Recent developments of the Middle East catalog, *Journal of Seismology*, 18, N4, 749-772, DOI 10.1007/s10950-014-9444-1, 2014. ... [3]

3.4 Georadar surveys

We used a georadar to explore the subsoil of the deformations detected on the surface. Due to the dense forest and steep slopes, the survey was conducted along the Jvari-Khaishi-Mestia road where it intercepts the two landslides. The georadar surveys were conducted using a Zond-12e Ground Penetrating Radar (GPR) equipment, which is a portable digital subsurface sounding radar that can be carried by a single operator. In the surveying process, the operator is getting real-time information comprising a GPS radiolocation profile. The GPR instrument works at single channel or double channel, in the time range from 1 to 2000 ns with 1 ns step. Frequency of pulse repetition of transmitter is 115 KHz with scan rate of 56 (for single channel system) or 80 (for double channel system). We used three different frequencies of the receiver-transmit antenna of 100, 300 and 500 MHz, some examples of which are shown in Figures 10 and 11. The surveys carried out at higher frequencies have good detail only in the very first meters of depth, whereas at lower frequencies the depth of investigation increases but with lower resolution.

Starting with the eastern landslide, a GPR 350-m-long survey has been carried out in a N-S sense along the road, intercepting several slip planes that deform the asphalt, and the main head scarp (Fig. 10A). In the section corresponding to 500 MHz (Fig. 10B), it is possible to observe several vertical to subvertical interruptions of the uppermost strata continuity. At these interruptions, strata show offsets of tens of centimeters, mostly on the southern block. Some of the discontinuities dip steeply southward, corresponding to a normal kinematics due to downsagging of the hangingwall block. Some strata at the northern (right) part of the section are tilted northward, in correspondence of the northernmost detected slip plane. This slip plane coincides in position with the northernmost main landslide slip surface. Its local southward dip and opposite tilting (i.e. northward) of strata are thus coherent with the border position of the structure. In the southern part of the section, strata are tilted southward. The GPR section corresponding to 300 MHz (Fig. 10C) shows the presence of the same discontinuities recognized in the 500 MHz section, indicating they really correspond to slip planes of the landslide that prolong at depth.

At the western landslide, it has been possible to carry out a GPR profile across one of the several active scarps affecting the Jvari-Khaishi-Mestia road (Fig. 11A). The profile trends E-W and is 14-m-long. In the section corresponding to 500 MHz (Fig. 11B), a zone of deformation is visible in the first meter of depth, which separates a dominion to the right (i.e. to the east) of undeformed horizontal strata with respect to a western dominion characterized by tilted strata. Resolution is not enough to observe offset of single strata, but the location of this vertical discontinuity coincides with the slip plane observed on the asphalt. In the 300 MHz and 100 MHz sections, a clear zone of offset strata is recognizable (Figs. 11C-D). Strata are tilted and downsagged, with offsets of tens of centimeters. Downsagged strata are located on the western block, with the slip plane steeply dipping westward, corresponding to a normal kinematics of the hangingwall block. This slip plane coincides in position with the plane of the 500 MHz section and the scarp surveyed in the field.

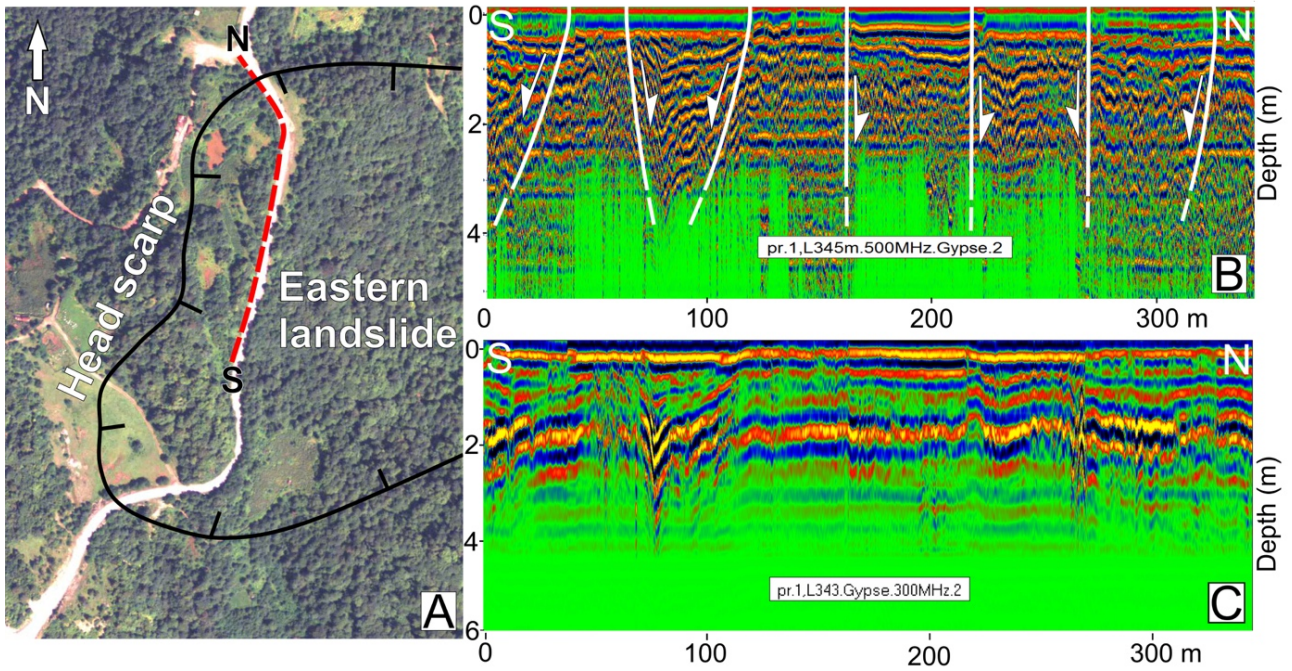


Figure 10: A. Location of the Ground Penetrating Radar (GPR) survey (red dashed line) carried out in the eastern landslide across several active slip planes affecting the main road. The black line shows the uppermost main head scarp of the landslide. GPR sections surveyed with an antenna at: B. 500 MHz, and C. 300 MHz. The 500 MHz section is interpreted with the main slip zones (white lines).

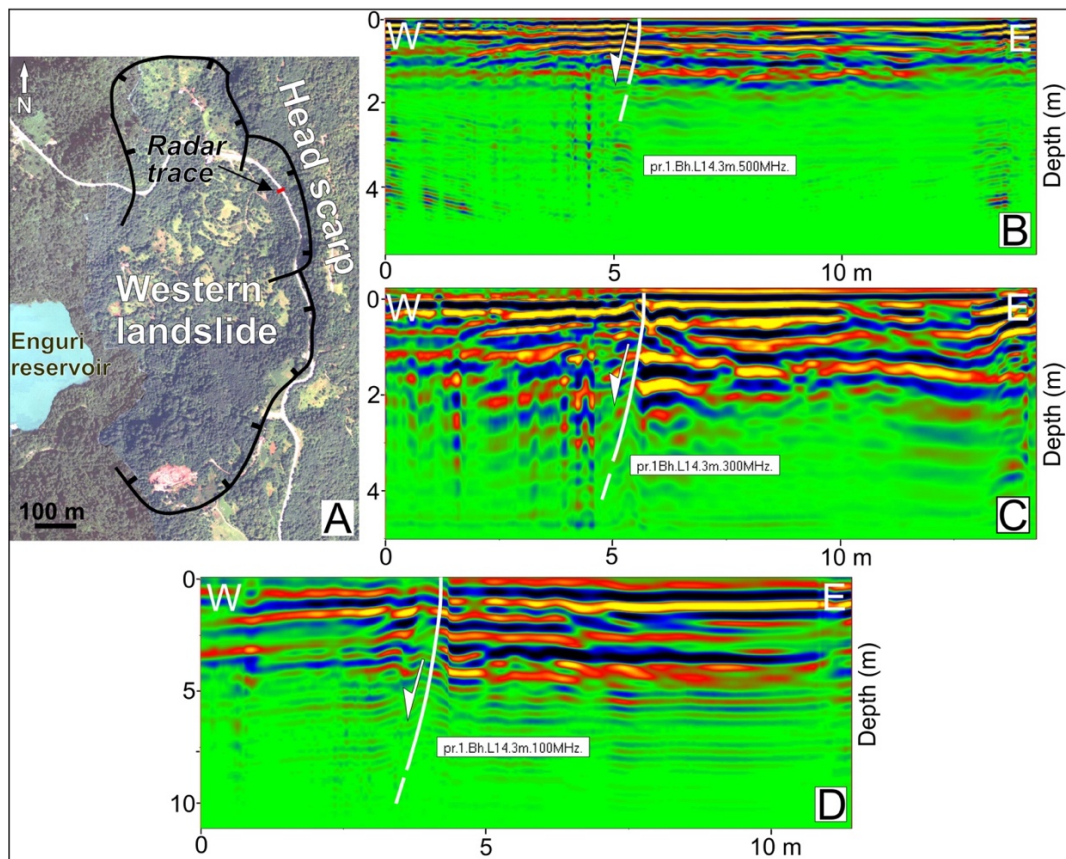


Figure 11: A. Location of the Ground Penetrating Radar (GPR) survey carried out in the western landslide across one of the active upper slip plane affecting the main road. The black line shows the uppermost head scarp of the

landslide. B. GPR sections surveyed with an antenna at: B. 500 MHz, C. 300 MHz, and D. 100 MHz. The white lines represent the same slip plane.

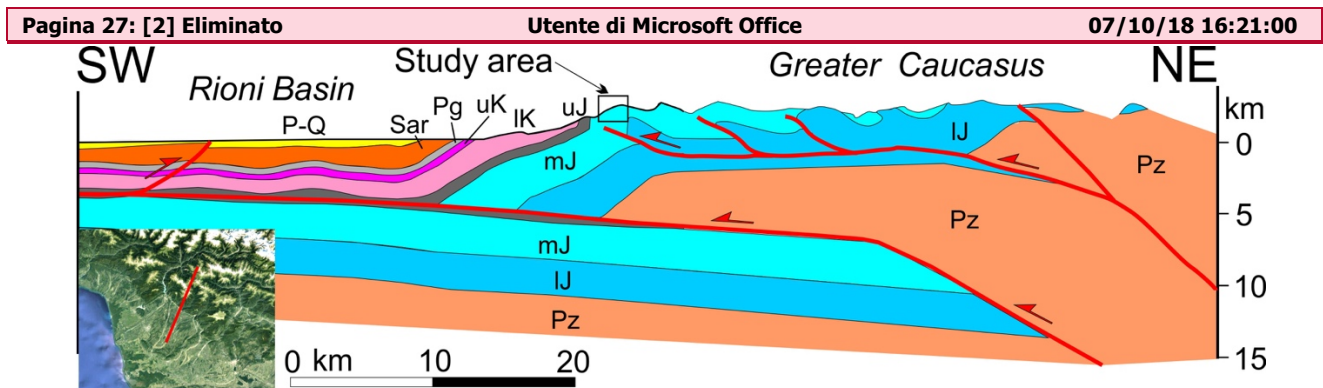


Figure 16: Structural section passing through the study area (box), obtained by integrating our field surveys with geophysical and geological data from Banks et al. (1997). Note the presence of a main basal thrust dipping north, which shows a ramp-flat geometry that produced a frontal asymmetric ramp anticline.

Pagina 36: [3] Eliminato	Utente di Microsoft Office	18/10/18 16:10:00
--------------------------	----------------------------	-------------------

Zare, M., Amini, H., Yazdi, P., Sesetyan, K., Demircioglu, M.B., Kalafat, D., Erdik, M., Giardini, D., Khan, M.A., and Tsereteli N.: Recent developments of the Middle East catalog, *Journal of Seismology*, 18, N4, 749-772, DOI 10.1007/s10950-014-9444-1, 2014.

Zare, M., Amini, H., Yazdi, P., Sesetyan, K., Demircioglu, M.B., Kalafat, D., Erdik, M., Giardini, D., Khan, M.A., and Tsereteli, N.: Reply to “comment on ‘recent developments of the Middle East catalog’”, *Journal of Seismology*, 21, 1, 269-271, 2017.